

University of Louisville

## ThinkIR: The University of Louisville's Institutional Repository

---

Electronic Theses and Dissertations

---

5-2024

### Investigation of Avaren-Fc's therapeutic potential against ovarian cancer.

Katarina Lee Mayer  
*University of Louisville*

Follow this and additional works at: <https://ir.library.louisville.edu/etd>



Part of the [Immunotherapy Commons](#), [Other Pharmacy and Pharmaceutical Sciences Commons](#), and the [Pharmaceutics and Drug Design Commons](#)

---

#### Recommended Citation

Mayer, Katarina Lee, "Investigation of Avaren-Fc's therapeutic potential against ovarian cancer." (2024). *Electronic Theses and Dissertations*. Paper 4331.  
<https://doi.org/10.18297/etd/4331>

This Master's Thesis is brought to you for free and open access by ThinkIR: The University of Louisville's Institutional Repository. It has been accepted for inclusion in Electronic Theses and Dissertations by an authorized administrator of ThinkIR: The University of Louisville's Institutional Repository. This title appears here courtesy of the author, who has retained all other copyrights. For more information, please contact [thinkir@louisville.edu](mailto:thinkir@louisville.edu).

INVESTIGATION OF AVAREN-FC'S THERAPEUTIC POTENTIAL  
AGAINST OVARIAN CANCER

By

Katarina Lee Mayer

B.S., University of Louisville, 2021

A Thesis Submitted to the Faculty of the University of Louisville School of Medicine in  
Partial Fulfillment of the Requirements for the Degree of

Master of Science  
in Pharmacology and Toxicology

Pharmacology and Toxicology

University of Louisville

Louisville, Kentucky

May 2024

Copyright 2024 by Katarina Lee Mayer

All rights reserved



INVESTIGATION OF AVAREN-FC'S THERAPEUTIC POTENTIAL  
AGAINST OVARIAN CANCER

By

Katarina Lee Mayer

B.S., University of Louisville, 2021

A Thesis Approved on

April 18<sup>th</sup>, 2024

By the following Thesis Committee

---

Dr. Nobuyuki Matoba

---

Dr. Leah Siskind

---

Dr. Kenneth Palmer

---

Dr. Sham Kakar

---

Dr. Sucheta Telang

---

Dr. Kavitha Yaddanapudi

## DEDICATION

This thesis is dedicated to my late grandfather, John Jacob Phillip Mayer, Jr., who  
always supported me.

## ACKNOWLEDGEMENTS

Thank you to Dr. Nobuyuki Matoba for the privilege to be a part of your lab. Your mentorship inspires me to be a better person and scientist each day. I am also thankful for the members of the Biopharmaceutical Research Unit, who have supported my development as a young researcher. Specifically, I would like to thank Dr. Noel Verjan-Garcia for the introduction into immunology and guidance in learning new techniques. I would also like to thank Matt Dent, Mickey Reeves, and Wendy Kittle for all the shared crosswords, laughs, and making the lab a warm and welcoming place.

Thank you to my family who has helped support me through this journey of scientific and self-discovery. Namely, thank you to my grandparents Gwendolyn and John Mayer and Nancy and Rick Belcher. You all have had an immeasurable impact on my life, and I cannot express my gratitude enough for everything you all have done for me. I would also like to thank Dr. Jade Daugherty for being a wonderful role model and a positive influence in all stages of my life. A final thank you is to my partner, Dylan Turner, whose unwavering support has played a vital role in making this project possible.

## ABSTRACT

### INVESTIGATION OF AVAREN-FC'S THERAPEUTIC POTENTIAL AGAINST OVARIAN CANCER

Katarina Lee Mayer

April 18<sup>th</sup>, 2024

This thesis describes the investigation of Avaren-Fc (AvFc), a novel lectin-based therapeutic fusion protein consisting of the recombinant Avaren lectin and the Fc region of human IgG1, against ovarian cancer. AvFc possesses selectivity toward tumor-associated *N*-linked high-mannose-type glycans. The present study demonstrates AvFc's *in vitro* activity against OVCA cell lines via antibody-dependent cell-mediated cytotoxicity and its ability to extend the survival of mice challenged with murine ID8 OVCA cells after repeated systemic administration. Furthermore, AvFc treatment in this model was found to increase the presence of peritoneal leukocytes, suggesting a shift toward an improved antitumor immune response. Another key finding of the current work was AvFc's preferential binding to primary human OVCA tumor tissue over healthy adjacent tissue. Overall, these results emphasize AvFc's therapeutic potential by effectively leveraging OVCA-associated high-mannose glycans as a target to induce cancer cell elimination.



## TABLE OF CONTENTS

DEDICATION .....	iii
ACKNOWLEDGEMENTS.....	iv
ABSTRACT .....	v
LIST OF TABLES .....	vii
LIST OF FIGURES .....	viii
CHAPTER 1: INTRODUCTION .....	1
Glycosylation in cancer .....	1
Anticancer lectins.....	3
Ovarian cancer .....	4
Avaren-Fc .....	7
Anticancer activity of Avaren-Fc.....	8
CHAPTER 2: METHODS AND MATERIALS.....	12
CHAPTER 3: RESULTS .....	25
Anti-Ovarian cancer activity of Avaren-Fc.....	25
CHAPTER 4: DISCUSSION .....	40
REFERENCES.....	49
CURRICULUM VITAE .....	54

## LIST OF TABLES

Table 1. Description of AvFc variants. ....	23
Table 2. Antibodies used in this thesis. ....	24
Table 3. Potential glycoprotein targets of AvFc. ....	31

## LIST OF FIGURES

Figure 1. Avaren-Fc's proposed anticancer mechanism via ADCC. ....	11
Figure 2. AvFc binds to and induces ADCC against a panel of OVCA cell lines. ....	30
Figure 4. Effects of AvFc in the ID8-Luc OVCA challenge model. ....	33
Figure 6. Immune cell profile of AvFc-treated, ID8-Luc-challenged animals. ....	36
Figure 7. Representative histology of ID8-Luc-derived tumor tissue. ....	37
Figure 8. Fluorescent IHC of AvFc binding to ID8-Luc-derived tumor tissue. ....	38
Figure 9. Conventional IHC of AvFc binding to human OVCA tissues. ....	39

## CHAPTER 1: INTRODUCTION

### **Glycosylation in cancer**

Glycosylation is a post-translational modification where a glycan, commonly known as a chain of carbohydrates, is enzymatically attached to a macromolecule to form a glycoconjugate [1]. Glycans are synthesized through a series of sequential modifications by glycosyltransferase enzymes located in particular organelle regions, which are also responsible for the initial transfer of monosaccharides from donor molecules to the acceptor sugars. The composition of glycans on the cell surface are also referred to as the glycocalyx.

In mammalian cells, one major class of glycoconjugates is glycoproteins, which can be generated through *N*- and *O*-glycosylation and respectively result in *N*- and *O*-glycosylated proteins [2]. *O*-glycosylation occurs at the reactive OH group of Ser and Thr residues through the attachment of 1,3-linked N-acetylglucosamine (GalNAc) or N-acetylglucosamine (GlcNAc), eventually resulting in mucin or non-mucin type *O*-glycans. In contrast to *O*-glycosylation, *N*-glycosylation takes place at a specific amino acid motif minimally comprised of Asn-X (any amino acid except Pro)-Ser/Thr. *N*-glycosylation can generate three different types of *N*-glycans: high-mannose, hybrid, and complex. In cancer, both processes are dysregulated, consequently modifying the attached glycans and impacting cellular functions, including cell growth, survival, and eventual metastasis [2, 3].

Of particular interest for this thesis is the cancer-induced change in *N*-glycosylation, since the disturbance of this cellular process has been shown to be highly

related to oncogenesis and metastasis; however, the specific mechanisms are yet to be fully understood [3]. In short, normal *N*-glycosylation is initiated in the endoplasmic reticulum (ER) by the creation of the lipid-glycan precursor (polyprenol dolichol pyrophosphate) attached to a core of two N-acetylglucosamines (GlcNAcs) decorated with mannose [1]. This highly mannosylated, branched structure is then flipped *en bloc* into the luminal space of the ER, where the oligosaccharyltransferase complex facilitates the transfer of the precursor glycan to a Asn-X-Ser/Thr motif of the target protein. At the end of processing in the ER, the glycan composition includes a total of nine mannose molecules attached to the core GlcNAcs (GlcNAc<sub>2</sub>Man<sub>9</sub>). The glycan is further processed within the Golgi apparatus where glycosidases and glycotransferases of the *cis*-Golgi will trim mannoses off to result in GlcNAcMan<sub>5</sub>, the last high-mannose type glycoform in this series of events. The subsequent addition of GlcNAc to the GlcNAcMan<sub>5</sub> structure forms a hybrid glycan, and upon further processing and maturation within the *medial*- and *trans*-Golgi, complex glycans will be created. The glycoproteins are then transferred to their target location by their insertion into the cell membrane or other necessary sites.

Within cancerous cells, *N*-glycosylation is influenced by various factors including altered expression of glycotransferases and glycosidases, as well as the availability of the donor sugars [4, 5]. In certain cancers, dysregulation of glycosylation pathways leads to an increased proportion of high-mannose type glycans, including ovarian cancer [6, 7], lung cancer [8], melanoma [9], cholangiocarcinoma [10], breast cancer [11], pancreatic cancer [12], and colorectal cancer [13]. The biological implications of increased *N*-linked high-mannose glycans are not well understood, but they are suspected to play a role in cancer cell migration and metastasis [7, 8, 10-12]. Overall, the alteration of the cancer cell glycocalyx, marked by an increase in *N*-linked high-

mannose glycans, provides a promising target for the development of new therapeutic interventions.

### **Anticancer lectins**

Lectins are a group of carbohydrate-binding-proteins of non-immune origin that can be found naturally in most kingdoms [14]. They are involved in a variety of biological processes, including cell signaling, defense against pathogens, and immune cell trafficking. Since the 1960s, advances in biotechnology have integrated lectins into methods such as chromatography, microarrays, and imaging (e.g., lectin blots, cytochemistry, and histochemistry). Additional research on the mechanisms of lectins revealed their recognition of diverse glycans and induction of cell death pathways like apoptosis and autophagy [14, 15]. To date, many high-mannose glycan-binding lectins have been identified and investigated for potential anticancer properties [16, 17]. The most well-known lectin, concanavalin A (conA) derived from *Cannavalia ensiformis* (commonly referred to as jack bean) was the first isolated lectin in 1919 [14]. ConA has been extensively characterized since its purification to identify its affinity toward high-mannose and its consequent induction of apoptosis or autophagy; a mechanism that has been advantageously applied toward broad anticancer applications *in vitro* and *in vivo* [18-21].

One such cancer that would benefit from lectin-based therapeutics is ovarian cancer (OVCA). In OVCA, high-mannose glycans aberrantly decorate malignant cells, and their increased presence in tumors is correlated with changes in early *N*-glycosylation enzymes in prior to the formation of hybrid type glycans [6, 7]. A lectin isolated from the seeds of *Dioclea lasiocarpa* with suspected mannose/glucose specificity, termed DLasiL, was shown to have antiproliferative effects against the A2780

human OVCA cell line *in vitro* and is hypothesized to induce caspase-mediated apoptosis [22]. The *Rhizoctonia bataticola* lectin has been shown to bind, induce apoptosis, and inhibit the migration of OVCA cell lines, as well as selectively recognize human OVCA tissues through more promiscuous binding toward *N*- and *O*-glycans associated with cancer antigen 125 (CA125) [23, 24]. Despite their promising *in vitro* activity, DLasiL and the *R. bataticola* lectin have yet to be evaluated for safety and efficacy in animal models of cancer. In fact, very limited studies have been conducted evaluating the anti-OVCA activity of lectins *in vivo*. The recombinant mistletoe lectin, specific to galactose (found in hybrid or complex *N*-glycans), has demonstrated efficacy in a human SoTu3 xenograft model of OVCA in severe combined immunodeficient (SCID) mice, as well as syngeneic murine models of various cancers [16, 25, 26]. This recombinant mistletoe lectin, referred to as avisumine or CY-503 in recent work, progressed to Phase II clinical trials for melanoma (NCT00658437) and metastatic colorectal cancer (NCT00932724) but has had no clinical advances since 2013. On a larger scale, the current list of Food and Drug Administration (FDA)-approved cancer drugs does not include lectins, likely due to their off-target effects and toxicity profile. Thus, there is ample room for the development and improvement of lectins as anticancer agents, particularly in the context of novel, targeted therapeutic strategies for OVCA treatment.

### **Ovarian cancer**

Ovarian cancer (OVCA) is the deadliest gynecological malignancy and the fifth leading cause of cancer death in females of all ages in the United States [27]. In 2024, the current 5-year survival rate is 51% with an estimated 12,740 deaths as a result of the disease [27]. Importantly, early diagnosis of OVCA can improve survival, as localized

OVCA has a 93% survival rate in comparison to distant, late stage OVCA with 33% survival, according to the National Cancer Institute Surveillance, Epidemiology, and End Results Program. OVCA encompasses stromal cell tumors, germ cell tumors, and epithelial ovarian carcinomas, which are classified based on tissue origin, histological subtype, and molecular features [28, 29]. Epithelial ovarian carcinomas originate from the epithelium of the ovary, fallopian tubes, or mesothelium and are the most common type of OVCA accounting for approximately 90% of diagnoses [28-30]. The category of epithelial ovarian cancer (EOC) includes clear cell, endometrioid, mucinous, and low and high grade serous ovarian carcinomas [29]. Initial suspicions of EOC are investigated by pelvic ultrasound and other imaging methods, like CTs or MRIs, to evaluate the potential landscape of EOC dissemination [31]. The staging of these tumors is surgically performed to evaluate the tumor characteristics based on criteria set forth by the International Federation of Gynecology and Obstetrics and the Union for International Cancer Control TNM (“Tumor”, “Node”, “Metastasis”) staging systems [32]. These guidelines describe stages I-IV of OVCA with detailed substages, defining stage I as an ovary-isolated tumor through stage IV as the metastasis outside of the peritoneum. Symptoms of EOC can contribute to late diagnosis as abdominal bloating and distension, nausea, fatigue, back pain, etc. are nonspecific to the disease. Efforts have been made to develop screening methods for EOC, such as serum CA125, however there is currently no approved approach for early detection [33].

The current first-line standard of care for EOC is debulking surgery followed by multiple cycles of chemotherapeutics [31, 34]. Surgery of low-grade tumors (stage IA) may provide patients with a chance for fertility conservation, whereas surgery of advanced stage EOC often includes a hysterectomy, bilateral salpingo-oophorectomy, and an omentectomy. Most patients will then receive a chemotherapeutic regimen



typically consisting of a taxane, like paclitaxel, and a platinum-based drug, such as carboplatin or cisplatin. The use of these chemotherapeutics may be effective for some, however approximately 70% of patients will face platinum-resistant disease recurrence within 3 years, rendering these drugs ineffective [34].

Standard second-line treatment strategies for patients with platinum-resistant disease include treatment with a nonplatinum chemotherapy, such as doxorubicin, or clinical trial enrollment [35]. Recent FDA approval of maintenance drugs, including poly ADP-ribose polymerase inhibitors and an anti-vascular endothelial growth factor monoclonal antibody (bevacizumab), have prolonged progression free survival but not overall survival [34]. Furthermore, the side effects of the approved drugs are deleterious to patient health as systemic doxorubicin administration is associated with significant cardiotoxicity [36]. Alternate formulations of doxorubicin, such as the liposomal formulation termed DOXIL, have managed to limit toxicity, but unfortunately have poor patient response rates of less than 20% [37]. Additionally, bevacizumab may cause bowel perforation among other adverse events that prevent its use in patients with disease recurrence [35]. Therefore, the current treatment options for EOC fail to effectively manage platinum-resistant disease recurrence. The introduction of immune checkpoint inhibitors has marginally improved EOC treatment, likely due to the lack of specificity toward EOC and the immunosuppressive tumor microenvironment established by EOC, but have yet to demonstrate significant clinical benefit [38, 39].

In EOC, the immune system is a major component in controlling tumor detection and growth [34, 40]. Together the leukocytes of the tumor and surrounding peritoneal fluid (ascites) orchestrate antitumor responses mediated by natural killer (NK) cells, cytotoxic CD8 T cells, Th17 T cells, and M1 macrophages. The increased presence of lymphocytes within the tumor is regarded as an important prognostic factor for

progression-free survival and overall survival [41]. However, in EOC the development of an immunosuppressive, protumor immune phenotype consisting of regulatory T cells, M2 macrophages, and exhausted NK and CD8 T cells is common and an unfortunate consequence of current cancer immunotherapies [40]. Therefore, the current treatment options for OVCA have yet to provide effective therapeutic approaches that are specific toward malignant cells and improve the antitumor immune response.

### **Avaren-Fc**

Our proposed drug candidate, Avaren-Fc (AvFc), is termed a “lectibody” based on its unique antibody-like structure, consisting of a novel recombinant lectin, Avaren, translationally fused to the Fc region of human IgG1 [42]. The Avaren lectin is a modified variant of the actinomycete-derived actinohivin, which binds the terminal  $\alpha$ 1,2-linked mannose of asparagine-linked high-mannose glycans and may bind up to three high-mannose glycans in its monomeric form [42-45]. Structure guided mutations introduced into actinohivin have enabled the Avaren lectin to be produced more efficiently in *Nicotiana benthamiana* in comparison to the parent actinohivin molecule, while maintaining its 3D conformation and glycan binding ability [42]. To further enhance the properties of the Avaren lectin, the Fc region of human IgG1 was translationally fused to two Avaren lectins in place of the fragment antigen binding (Fab) region, which is comprised of a heavy and light chain. This fusion protein was created with the goal of increasing the avidity of the Avaren lectin through dimerization, prolonging the *in vivo* half-life, and providing Fc-mediated effector functions, such as antibody-dependent cell-mediated cytotoxicity (ADCC), antibody-dependent cell-mediated phagocytosis (ADCP), and complement-dependent cytotoxicity. Furthermore, unlike many other exogenous mannose-binding lectins reported to date, the AvFc lectibody does not exhibit

undesirable mitogenicity or direct cytotoxicity against normal cells *in vitro* and has shown no signs of toxicity *in vivo* using mice, rats, and rhesus macaques [42, 46, 47].

### **Anticancer activity of Avaren-Fc**

Our original intention was to develop AvFc as an antiviral against enveloped viruses displaying high-mannose glycans, such as HIV [42, 48] and HCV [46]. However, emerging evidence that many types of cancer cells also aberrantly display these glycans led us to explore the potential anticancer activity of AvFc. Recent studies by Oh, et al. (2022) and Dent, et al. (2022) have documented the anticancer activity of AvFc and the key points will be described in this section.

The foundational work by Oh, et al. (2022) showed that AvFc binds to panels of established human cancer cell lines from various tissue origins at low nanomolar concentrations and selectively recognizes primary human lung tumor tissues over healthy adjacent tissues. This interaction was found to be dependent on the presence of high-mannose glycans, as demonstrated by the lack of AvFc binding to A549 lung cancer cells when treated with endoglycosidase H, an enzyme that cleaves the bond within the chitobiose core of the high-mannose glycan, cleaving the branched glycan structure from the N-acetylglucosamine (GlcNAc) attached to the Asn residue of the protein. Specific glycoprotein targets of AvFc were isolated using a pull-down assay with A549 and H460 non-small cell lung cancer (NSCLC) cell lysates, compared to a non-sugar binding AvFc mutant serving as a negative control. This AvFc variant, termed AvFc<sup>Δlec</sup>, contains three-point mutations (Y32A, Y70A, and Y108A) within the Avaren lectin, effectively eliminating the lectin's glycan binding affinity (Table 1). Proteomics analysis via mass spectrometry identified a panel of glycoproteins uniquely recognized by AvFc, including epidermal growth factor receptor (EGFR) and insulin-like growth

factor 1 receptor (IGF1R). Upon binding to A549 and H460 NSCLC cells, AvFc induced ADCC (Figure 1) and inhibited EGFR and IGF1R signaling. The latter resulted in the inhibition of cell migration through the AKT and MAPK pathways in both cell lines. This result contrasts with the FDA-approved anti-EGFR monoclonal antibody cetuximab, which only inhibited migration in A549 cells treated with epidermal growth factor, highlighting the broader antitumor activity of AvFc. These antitumor effects observed *in vitro* have *in vivo* relevance, as demonstrated by a 6-dose regimen of 25 mg/kg of AvFc, which delayed tumor growth in both A549 and H640 subcutaneous xenograft challenge models and decreased tumor burden in the A549-GFP metastasis model. This work investigating AvFc against lung cancer presented promising results, demonstrating potent antitumor activity *in vitro* and *in vivo*. These findings justify further development of AvFc for additional cancer types that aberrantly display high-mannose glycans.

In our laboratory, AvFc is typically produced in a glycoengineered transgenic *N. benthamiana* line that lacks plant-derived  $\alpha(1,3)$ -fucose and  $\beta(1,2)$ -xylose glycans [49]. The work by Dent, et al. (2022) underscored the importance of using this glycoengineered *N. benthamiana* to fully harness the Fc-mediated antitumor functions of AvFc. In this study, an aglycosylated lectin body variant, termed AvFc<sup>Agly</sup>, was generated through a single point mutation (N200Q) in the *N*-glycosylation site located within the C<sub>H2</sub> domain of Fc region (Table 1). This served as a negative control for Fc-mediated functions. The study also compared AvFc expressed in the glycoengineered transgenic *N. benthamiana* and AvFc<sup>WT</sup>, which was expressed in wild-type *N. benthamiana*.

The Avaren lectin portion of AvFc, AvFc<sup>WT</sup> and AvFc<sup>Agly</sup> retained their cancer cell binding properties, as evaluated by a HIV gp120-capture ELISA and flow cytometric binding to B16F10 murine melanoma cells. Surface plasmon resonance analysis showed that AvFc, in comparison to AvFc<sup>WT</sup>, had a significant increased affinity toward

human Fcγ receptors (FcγRs) I and IIIa, as well as mouse FcγRIV, the murine analog of human FcγRIIIa. AvFc also demonstrated superior potency and a lower half maximal effective concentration (EC<sub>50</sub>) compared to AvFc<sup>WT</sup> in a reporter-cell-based ADCC assay using B16F10 cells (Figure 1). Furthermore, 6 doses of 25 mg/kg AvFc exhibited potent antitumor activity, significantly delaying tumor growth in both metastatic and flank tumor models of B16F10 melanoma. Interestingly, a separate B16F10 flank tumor challenge experiment demonstrated that pretreatment of mice with 6 doses of 25 mg/kg AvFc before flank tumor challenge followed by a 6-dose treatment regimen, significantly prolonged median survival relative to the group that received only the treatment doses. The contribution of AvFc pretreatment to prolonged survival is thought to be through the generation of antidrug antibodies (ADAs); however, the comparison of ADA titers between the group that received pretreatment and treatment with AvFc and the group that received AvFc treatment alone was nonsignificant. While the relationship between prolonged survival and AvFc pretreatment remains unclear, the data suggest that the ADAs against AvFc did not negate its efficacy. Overall, this work demonstrates the importance of glycoengineering in enhancing the potency and efficacy of AvFc.

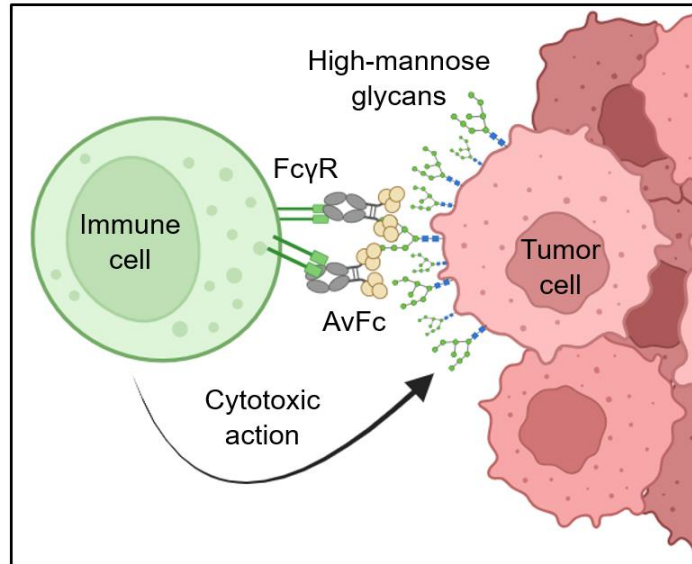


**Figure 1. Avaren-Fc's proposed anticancer mechanism via ADCC.** Tumor cells decorated with *N*-linked high-mannose type glycans are selectively bound by Avaren-Fc (AvFc). Circulating immune cells bearing Fcγ receptors (FcγR) recognize and bind to AvFc by its human IgG1 Fc region. This crosslinking causes downstream signaling of FcγRs with immunoreceptor tyrosine-based activation motifs, such as FcγRIIIa on natural killer cells, resulting in the induction of antibody-dependent cell-mediated cytotoxicity (ADCC). ADCC mediates cell killing through the release of cytotoxic granules containing perforin and granzymes that lead to tumor cell apoptosis.

## CHAPTER 2: METHODS AND MATERIALS

### **Animal studies**

Studies involving animals were conducted under the approval of the University of Louisville Institutional Animal Care and Use Committee (IACUC protocols 21910, 20714, and 23305). All animals were housed in a temperature- and humidity-controlled environment, with an alternating 12-hour day/night cycle. Animals were acclimated to the facility for one week prior to the start of each study and provided a standard diet and water *ad libitum*.

### **Plant growth**

*Nicotiana benthamiana* plants were grown in a temperature-controlled room with lighting set to a 16/8-hour day/night cycle. Three to five seeds were placed into pots containing damp soil and were covered with plastic wrap to germinate. After 12 days, seedlings were thinned to one per pot to promote plant growth. Plants were fertilized with Peters Peat-Life Special 17-3-17 (nitrogen-phosphate-potash) fertilizer diluted in water three days a week for four weeks before agroinfiltration.

### **Expression and purification of Avaren-Fc and its variants**

AvFc<sup>Δlec</sup>, and AvFc<sup>Δgly</sup> were expressed in wild type *N. benthamiana* plants. AvFc was expressed in the glycoengineered line of *N. benthamiana*, which was generated by RNA interference (RNAi) knockdown of β1,2-xylosyltransferase and α1,3-fucosyltransferase glycotransferase enzymes (provided by Dr. Herta Steinkellner at

University of Natural Resources and Life Sciences, Vienna, Austria; [49]), referred to as ΔXF plants in this thesis (Table 1). The post-transcriptional silencing of these glycosylation enzymes prevents the respective addition of xylose to the core mannose and fucose to the N-acetylglucosamine (GlcNAc) core of the GnGn glycoform, essentially preventing the formation of plant-specific *N*-glycans on the recombinant proteins. The plants were agroinfiltrated with *Agrobacterium tumefaciens* (GV3101) transformed with magnICON® vectors for recombinant protein expression of the desired lectin variant. This magnICON® technology employs a deconstructed tobacco mosaic virus vector system for transient overexpression *in planta* through the incorporation of three essential modules, including the 5' promoter elements, the 3' elements with the gene of interest (i.e., AvFc and its variants), and integrase to fuse the 5' and 3' to form an RNA-based replicon for expression of the gene of interest in the leaf tissue.

Agroinfiltration began with a culture of *A. tumefaciens* transformed with the desired construct plasmid in 150 mL of LB medium containing rifampicin and carbenicillin or kanamycin, depending on the construct. Cultures were incubated overnight at 30°C with shaking at 150 rpm. The agrobacteria were collected through centrifugation at 7000xg for 15 minutes, after which the media was decanted and the pellet resuspended in MES agroinfiltration buffer (10 mM MES hydrate, 10 mM MgSO<sub>4</sub> heptahydrate, pH 5.5). The optical density at 600 nm (OD<sub>600</sub>) was obtained for the bacteria solution using a Nanodrop One C (Thermo Scientific) and diluted to 0.1 into 2 L of agroinfiltration buffer. Plants were agroinfiltrated using the vacuum method where plants are inverted and submerged in the bacteria-containing buffer. The desiccator is then held under a vacuum for two 3-minute intervals before swiftly repressurizing to promote buffer uptake through the stomata and into the interstitial space of the plant. The infiltrated plants were returned to the growth room for 7 days and cared for as previously mentioned.



Extraction of crude AvFc product was initiated seven days post-infiltration when infected leaf tissue was harvested, weighed, and homogenized in a 2:1 ratio of extraction buffer (10 mM NaPi, 40 mM ascorbic acid, pH 6.8): gram of leaf tissue. The extract was passed through a layer of cheese cloth and miracloth, before adjusting the pH of the crude extract to 6.8 and subsequently clarifying by centrifugation at 15,000xg for 15 minutes at 4°C. The clarified supernatant was then decanted, adjusted back to a pH of 6.8, and filtered using a 0.2 µm vacuum filter. Filtered extract was then loaded onto a protein A column using the AKTA pure™ fast protein liquid chromatography (FPLC) system. Once the sample was applied to the column, the unbound material was washed away with 10 column volumes of 5 mM NaPi (pH 6.8). The bound material was eluted using 10 column volumes of 2 M arginine (pH 3) in a single step and collected in 10 mL fractions and neutralized with 3 M tris base (pH 9).

Protein-containing fractions, as determined by the spectrophotometer of the FPLC, were concentrated using Amicon® ultra centrifugal filters with a 30 kDa molecular weight cut off (MWCO) and diluted 20x with 5 mM NaPi (pH 6.8). The diluted sample was then applied to a ceramic hydroxyapatite type II (CHTII) column and subsequently washed with 10 column volumes of 5 mM NaPi (pH 6.8). Bound material was eluted with a gradient of 5 mM NaPi to 5 mM NaPi with 1 M NaCl (pH 6.8) over 10 column volumes and collected in 40 mL fractions. The column was stripped using 2 column volumes each of water, 250 mM NaPi (pH 6.8), water, and stored in 0.1 M NaOH. SDS-PAGE confirmed the fractions containing the lectibody using an AvFc reference standard. Fractions containing protein were then concentrated using Amicon® ultra centrifugal filters with a 30 kDa MWCO and buffer exchanged into AvFc formulation buffer (40 mM histidine, 100 mM sucrose, 100 mM NaCl, pH 7.4). Product then underwent endotoxin removal by phase separation with Triton-X114 as described below.

### **Endotoxin removal by phase separation**

Endotoxin was removed from AvFc product by phase separation with 1% Triton-X114 v/v, a 15-minute incubation on ice, followed by a generous vortex and a 10-minute incubation in a 37°C water bath. After the water bath, the sample was evenly aliquoted into 1.7 mL tubes and centrifuged at 22,000xg at 37°C for 20 minutes. The product-containing supernatant was removed and placed in a new tube, being careful to not disturb the bottom detergent layer. This process was repeated once more before detergent removal.

Residual Triton-X114 was removed with Pierce™ spin columns (Thermo Fisher Scientific) through the addition of the sample, vortexing to promote resin interaction with the product, and allowing a residence time of 15 minutes before centrifugation at 1000xg for 3 minutes. The collected product was then diafiltrated with a minimum of 3x the sample volume of AvFc formulation buffer and concentrated with Amicon® ultra centrifugal filters with a 30 kDa MWCO. The product was then 0.2 µm syringe filtered and subsequently diluted in β-glucan blocking buffer for endotoxin testing using an Endosafe® nexgen-PTS™ (Charles River Laboratories) and determined to be endotoxin-free and stored at -80°C.

### **Cell culture**

All cell lines were housed in an incubator at 37°C with 5% CO<sub>2</sub>. B16F10, CAOv3, SKOV3, SW616 cell lines were purchased from the American Type Culture Collection (ATCC) and cultured in Dulbecco's Modified Eagle Medium (DMEM) with L-glutamine and sodium pyruvate, supplemented with 10% fetal bovine serum (FBS) and 1X penicillin/streptomycin. The Jurkat engineered T cell line, expressing human FcγRIIIa that induces NFAT-mediated luciferase expression, were purchased from Promega and maintained per the manufacturer's instructions. The ID8, ID8-VEGF-Defb29 and ID8-

Luciferase cell lines were gifts from Dr. Steve Fiering at the Geisel School of Medicine at Dartmouth University and Dr. Zong Seng Guo at the University of Pittsburgh School of Medicine. ID8 cells were maintained in DMEM with L-glutamine and sodium pyruvate, supplemented with 4% FBS, 1X penicillin/streptomycin, and 1X insulin-transferrin-selenium solution. ID8-Luciferase cells were cultured with the addition of 1 ug/mL blasticidin. Cells used in animal studies were verified to be mycoplasma free from IDEXX BioAnalytics and to further prevent contamination, Normocin™ from Invivogen was added to the culture medium per the manufacturer's protocol.

### **Flow cytometry to evaluate AvFc binding to cancer cells**

Cancer cells of interest were harvested and aliquoted to  $1 \times 10^6$  cells/sample. Cells were stained with AvFc at 1.5, 15, and 150 nM in flow cytometry staining buffer from eBioscience, detected using a 1:200 dilution of a goat anti-human IgG FITC secondary antibody (Table 2), and fixed using 10% buffered formalin. Experimental controls included samples stained with 150 nM AvFc<sup>Δlec</sup>, unstained cells with secondary detection only, and cell alone samples. Flow cytometry was performed using a BD FACSCalibur and the data analyzed in the FlowJo™ Software to determine the proportion of FITC+ cells, or cells positive for AvFc binding.

### **Antibody-dependent cell-mediated cytotoxicity assay**

Target cells were plated at 10,000 cells/well in a white 96-well plate in whole medium and incubated overnight at 37°C with 5% CO<sub>2</sub> to permit cell attachment. The following day, AvFc or AvFc<sup>Δgly</sup> were serially diluted (1:5) from 650 nM in RPMI 1640 medium, supplemented with 1% ultra-low IgG FBS from VWR and added to the target cells. The human FcγRIIIa-expressing Jurkat effector cells were collected, resuspended in the same media, and plated at 150,000 cells/well to provide an effector:target cell ratio

of 15:1. The target cells, drug, and effector cells were then incubated overnight at 37°C with 5% CO<sub>2</sub>. Notably, each plate contained controls that did not include drug, effector cells (target cells alone), or either (media alone). The final day of the assay, half the culture media was removed before the addition of the britelite plus reagent from the PerkinElmer Britelite Plus Reporter Gene Assay System. Luminescence was measured using a BioTek plate reader within 15 minutes. Fold luminescence induction was calculated from the ratio of relative luminescence units (RLUs) of the drug and the average RLU of the no drug control, normalized by the average RLU of the target cell controls. In GraphPad Prism, fold luminescence was plotted against the log concentration of drug and fit with a 4-parameter non-linear regression to determine EC<sub>50</sub>.

### **Identification of potential glycoprotein targets of AvFc**

Co-immunoprecipitation was performed using the Pierce Co-Immunoprecipitation Kit (Thermo Scientific) per the kit instructions to capture and isolate glycoprotein binding partners of AvFc from cell lysates of one murine OVCA (ID8) and two human OVCA (SKOV3 and SW626) cell lines. Cells were cultured in a 75 cm<sup>2</sup> flask before lysis with the kit's lysis buffer (1% NP-40, 10 mM EDTA) and 1X Halt™ protease and phosphatase inhibitor (Thermo Scientific). Lysate was then centrifuged to pellet the cell debris. Next, the lysate was precleared using an unconjugated agarose resin to remove proteins that would nonspecifically bind to the resin. The precleared lysate was then incubated with the AvFc- or AvFc<sup>Δlec</sup>- conjugated agarose resins in capped spin tubes overnight at 4°C with gentle end-over-end mixing. The next day, the mixture in the spin tube was washed 5 times with the manufacturer provided wash buffer before elution of the bound proteins using a low pH buffer. Up to eight elutions were performed, or until no protein was detected in three subsequent fractions by A280 using a Nanodrop One C (Thermo

Scientific). The protein containing eluate was combined and neutralized with 1 M tris base before submission to the proteomics core at the University of Louisville.

At the proteomics core, the samples were prepared through reduction, alkylation, and trypsin digestion before separation by electrospray ultra-high performance liquid chromatography-mass spectrometry (UHPLC-MS). Protein identification was conducted in Scaffold proteome software where the data was filtered to control for false discovery rates using PeptideProphet and ProteinProphet algorithms (Institute for Systems Biology). Accepted identification of proteins was at >95% probability by PeptideProphet and ProteinProphet algorithms. Once identified, protein abundance was compared in Scaffold by normalizing the total spectra or the intensity based absolute quantification (iBAQ) method. To further filter the results, Gene Ontology (GO) terms were used to determine the proteins bound by AvFc through excluding AvFc<sup>Δlec</sup>-captured proteins. The identified, AvFc-specific proteins were further characterized by the number of potential *N*-glycosylation sites using the NetNGlyc server (Technical University of Denmark) and the unique protein-associated UniProt accession number.

### **Immunocytochemistry of cancer cells**

Immunocytochemistry was performed to generate preliminary data in the confirmation of AvFc glycoprotein targets identified by co-immunoprecipitation and proteomics analysis. The human OVCA cell line, SKOV3, was cultured in a 75 cm<sup>2</sup> flask and harvested using 10 mM EDTA. Cells were washed once with culture medium before seeding 2.5 x 10<sup>5</sup> cells/well in a 4-chambered microscope slide in 1 mL complete medium. The cells were incubated overnight at 37°C with 5% CO<sub>2</sub> to allow the cells to adhere to the slide. After confirming the cells have adhered, the wells were washed twice with PBS and the slides fixed in methanol at -20°C for 5 minutes.

Fixed slides were rehydrated in PBS prior to blocking of Fc receptors with 10% FBS and mouse  $\gamma$  globulin (20 ug/mL) and staining with 2 ug/mL of mouse anti-IGF2R, goat anti-mouse IgG AlexaFluor-594, AvFc, and goat anti-human IgG FITC (Table 2). Between each step, slides were washed three times in clean PBS. After the final wash, slides were mounted with *in situ* mounting medium with DAPI (Sigma Aldrich) and imaged using a Nikon AR inverted confocal microscope.

### **Syngeneic ID8-Luciferase OVCA challenge model**

The orthotopic ID8-Luciferase (ID8-Luc) challenge model was conducted with ID8-Luc cells that express luciferase, which can be utilized to measure *in vivo* tumor burden by bioluminescent imaging. This syngeneic OVCA model utilizes 8-week-old female C57Bl6 mice, given that OVCA is a gynecological cancer. On day 0,  $2 \times 10^6$  ID8-Luc cells were intraperitoneally (i.p.) injected in 200  $\mu$ L sterile PBS and permitted to establish tumors for 1 week. Starting on day 7, AvFc (25 mg/kg) or vehicle (AvFc formulation buffer, 100 mM sucrose, 100 mM sodium chloride, 40 mM histidine pH 7.4) was administered every other day (Q2D) through day 35. Disease progression was monitored by body weights, abdomen circumference, and bioluminescent imaging. Imaging took place at the University of Louisville's *In vivo* Molecular Imaging Core using the PhotonImager Optima (Biospace Lab) and analyzed with the M3Vision software (Biospace Lab). The images were taken 10 minutes after i.p. administration of 150 mg/kg luciferin for substrate distribution and signal generation. Humane endpoints of euthanasia were met if the animal reached 35 g or was moribund. In this model, the primary endpoint gauging drug activity was survival. Kaplan-Meier curves were generated in GraphPad Prism and statistically compared with the Gehan-Breslow-Wilcoxon test. Analysis of bioluminescent imaging data was conducted using a Kruskal-Wallis test with Dunn's multiple comparisons test.

### **Immune cell profiling of the murine ID8-Luc OVCA model**

Immune cell profiling was performed with the leadership of Dr. Noel Verjan-Garcia, who helped in the isolation and staining of immune cells, gating of cell populations, and data analysis. In the first experiment elucidating the immunomodulation caused by the ID8-Luc cells, animals were challenged with  $3 \times 10^6$  ID8-Luc or a PBS control on day 0 and treated with AvFc formulation buffer (vehicle) starting from day 7 to 35. Animals were euthanized after five weeks when the spleen and peritoneal lavage was used in flow cytometry for analysis of immune cell populations. Tumors were also cryopreserved for immunohistochemistry. In the second experiment evaluating the impact of AvFc treatment in the syngeneic ID8-Luc OVCA model,  $3 \times 10^6$  ID8-Luc cells were i.p. injected on day 0 and treated with AvFc (25 mg/kg) or vehicle starting on day 7 to 19. Animals were sacrificed after 7 doses of AvFc or vehicle, when the peritoneal lavage was used in flow cytometry and tumors were harvested for histology.

Splenocytes were isolated by mincing the spleens in RPMI-1640 with subsequent filtering through a 40  $\mu$ m cell strainer. The splenocyte suspension was then treated with ammonium–chloride–potassium (ACK) lysis buffer to lyse red blood cells via an increase in osmotic pressure. Samples were then centrifuged and washed with flow cytometry staining buffer (10% FBS, 10 mM HEPES, 10 mM EDTA, and 1 mM sodium pyruvate in PBS) to separate out cell debris for both the splenocyte and peritoneal fluid samples. Cells in all samples were counted and Fc receptors were blocked with mouse  $\gamma$  globulin (20  $\mu$ g/mL) and incubated on ice. Next,  $1 \times 10^6$  cells from each sample were seeded into a 96-well plate and washed with staining buffer three times. After the final wash, cells were resuspended and incubated in staining buffer containing a cocktail of fluorescent antibodies, specific to three panels: 1) myeloid cells, 2) T cells, and 3) natural killer and B cells (Table 2). All samples were then washed with staining buffer three times and

resuspended with 7-amino-actinomycin D (7AAD) viability dye for dead cell exclusion. Stained cells were then transferred into sample tubes, vortexed to ensure single cell suspensions, and acquired on a BD LSRFortessa™ using the BD FACSDiva™ Software.

Cell gating was performed in the FlowJo™ Software to identify specific cell populations named in Figures 5 and 6. General gating strategies were as follows: cell debris was excluded from whole cells, whole cells were gated to include live (7AAD-) cells, and further gated by specific markers dictated by the respective panel. Once the proportion of cell populations were identified in FlowJo™, samples were standardized to each animal using the sample cell count determined at time of cell isolation ((sample cell count \* proportion) / 100 = number of cells within the animal). For two experimental groups, an unpaired t-test was performed with a  $p < 0.05$  deemed to be significant. For three experimental groups, a Kruskal-Wallis test with Dunn's multiple comparisons was conducted with an adjusted  $p < 0.05$  threshold to determine significance between groups.

## **Histology**

Tumors were removed and fixed with 10% neutral buffered formalin for 24 hours and stored in 70% ethanol until tissue processing (Eprelia™ STP 120 Tissue Processor) and paraffin embedding (Eprelia™ Histostar™ Embedding Workstation). The tissue-containing blocks were then cut into 10  $\mu\text{m}$  thin sections for hematoxylin and eosin (H&E) staining (Eprelia™ Gemini™ AS Automated Slide Stainer).

## **Fluorescent immunohistochemistry of murine tumor tissue**

Tumor tissue was cryopreserved in Tissue-Tek® O.C.T. Compound and cut into 7  $\mu\text{m}$  thin sections for fluorescent immunohistochemistry (IHC). Slides were fixed in methanol at  $-20^{\circ}\text{C}$  for 5 minutes before storage. Stored slides were rehydrated in PBS



followed by blocking of Fc receptors with 10% FBS and mouse  $\gamma$  globulin (20  $\mu\text{g}/\text{mL}$ ) and staining with 2  $\mu\text{g}/\text{mL}$  of AvFc, goat ant-human IgG FITC, anti-E-cadherin AlexaFluor-647, and anti-Ki-67 AlexaFluor-594 (Table 2). Between each step, slides were washed three times in clean PBS. After the final wash, slides were mounted with *in situ* mounting medium with DAPI (Sigma Aldrich) and imaged using a Nikon AR inverted confocal microscope.

### **Conventional immunohistochemistry of human tissues**

IHC was performed on Ventana Discovery Ultra automated immunostainer (Ventana Medical Systems, Tucson, AZ). On-board antigen retrieval was performed with CC1 (pH 8.0) for 56 minutes at 95°C (Cat #950-124). Biocare Background Sniper was used for the blocking reagent (Cat #BS966, Biocare) for 4 minutes and endogenous peroxidase was blocked by Discovery inhibitor (Cat #760-4840, Ventana) for 4 minutes. 5.0  $\mu\text{g}$  of the primary antibody was tagged with digoxigenin using a Biocare Human-on-Human HRP-Polymer kit according to the manufacturer's instructions (Cat #BRR 4056K, Biocare). The tagged antibody was applied at a dilution of 1:100 and incubated for 36 minutes at 37°C. Mouse anti-Digoxigenin from the Biocare kit was applied as the secondary antibody for 12 minutes at 37°C. This was followed by Anti-Mouse HQ (Cat #760-4814, Ventana) for 12 minutes at 37°C and Anti-HQ HRP (Cat#760-4820, Ventana) for 12 minutes at 37°C. Visualization was performed using ChromoMap DAB (Cat #760-159, Ventana). Nuclear counterstaining was applied with Ventana Hematoxylin II for 12 minutes followed by a Bluing reagent for 8 minutes. Slides were dehydrated, cleared, and mounted as in routine processing.

AvFc variants	Variant description	Impact on function
AvFc	Expressed in glycoengineered <i>N. benthamiana</i> ΔXF plants, resulting in a “humanized” Fc region that lacks plant-specific glycoforms occupying the <i>N</i> -glycan site of the C <sub>H</sub> 2 domain.	High ADCC activity
AvFc <sup>Δlec</sup>	Three point mutations (Y32A, Y70A, and Y108A) within the Avaren lectin. Used as a negative control.	Unable to bind high-mannose glycans
AvFc <sup>Δgly</sup>	One point mutation (N200Q) within the <i>N</i> -glycan site of the C <sub>H</sub> 2 domain of the Fc region, preventing <i>N</i> -glycosylation. Used as a negative control.	Unable to elicit Fc-mediated effector functions

**Table 1. Description of AvFc variants.** All AvFc variants used in this thesis are defined and described above.

Antibody	Manufacturer	Catalog number
anti-CD19 APC	eBioscience	17019382
anti-CD3 FITC	eBioscience	11003282
anti-NK1.1 BV-605	BioLegend	1087396
anti-CD49b PE	eBioscience	12597181
anti-CD11b APC-Cy7	BioLegend	101225
anti-CD107a AlexaFluor-700	BioLegend	121627
anti-NKp46 BV-650	BioLegend	137635
anti-CD16.2 PE-Dazzle-594	BioLegend	149519
anti-CD11c PE	BioLegend	117308
anti-MHCII (IA-IE) BV-421	BioLegend	107631
anti-F4/80 PE-Cy7	eBioscience	25480182
anti-Ly6G APC	BioLegend	127614
anti-Ly6C AlexaFluor-700	BioLegend	128024
anti-CX3CR1 BV-605	BioLegend	149027
anti-CD206 BV-650	BioLegend	141723
anti-CD103 PE-Dazzle-594	BioLegend	156909
anti-CD86 PE-Dazzle-594	BioLegend	105041
anti-CD45 FITC	BioLegend	103108
anti-CD45R/B220 APC	BioLegend	103212
anti-CD25 AlexaFluor-700	BioLegend	102028
anti-CD4 BV-605	BioLegend	100512
anti-CD8a BV-650	BioLegend	100712
anti-CD62L APC-Cy7	BioLegend	104428
anti-TCR $\beta$ PE-Cy7	BioLegend	109222
anti-E-cadherin AlexaFluor-647	BioLegend	147308
Mouse anti-hIGF2R	RnD Systems	MAB2447
anti-mouse IgG AlexaFluor-594	BioLegend	405326
Goat anti-human IgG FITC	Abcam	ab98529
anti-Ki-67 AlexaFluor-594	BioLegend	151214

**Table 2. Antibodies used in this thesis.** All antibodies and their manufacturer information are listed above.

## CHAPTER 3: RESULTS

### **Anti-Ovarian cancer activity of Avaren-Fc**

We first evaluated AvFc's binding to OVCA cell lines by flow cytometry using mouse ID8 and ID8-VEGF-Defb29, in addition to human A2780, CAOV3, SKOV3, and SW626 cell lines. AvFc appeared to bind to the cancer cell surface in a high-mannose glycan-dependent manner, as indicated by the lack of binding observed with the non-sugar-binding mutant, AvFc<sup>Δlec</sup> (Figure 2A). AvFc demonstrated >90% saturation binding to both ID8 and ID8-VEGF-Defb29 at 15 nM, while achieving 50% saturation at 150 nM for all tested cell lines.

To understand the mechanism of selectivity behind AvFc binding, we aimed to identify potential glycoprotein targets of AvFc. To do so, we performed co-immunoprecipitation through incubating AvFc- or AvFc<sup>Δlec</sup>-conjugated agarose resins with cell lysates to isolate target glycoproteins. The co-immunoprecipitated glycoproteins were identified by electrospray ultra-high performance liquid chromatography-mass spectrometry (UHPLC-MS) and proteomics analysis to filter integral membrane proteins from other cytoplasmic and organelle proteins. Cell lysates of human ovarian, lung, and blood cancer cells were used, including the following cell lines: SKOV3, SW626, A549, H460, K562, and HL60. Additionally, cell lysate of the murine ID8 OVCA cell line was used. In comparison to AvFc<sup>Δlec</sup>, AvFc-specific glycoproteins were identified and further characterized by the number of potential *N*-glycosylation sites using the NetNGlyc server (Table 3). Overall, AvFc bound to glycosylated receptors, transporter proteins, and integrins. Across the SKOV3 and SW626 human and ID8 mouse OVCA cell lines, AvFc

commonly bound to epidermal growth factor receptor (EGFR, Egfr). This finding aligns with the work of Oh et. al (2022), which confirmed EGFR as a glycoprotein target in A549 and H460 NSCLC cell lines as well as primary human lung tumors [50]. A second common target among the OVCA cell lines was plexin-B2 (PLXB2, Plxnb2), a glycosylated receptor implicated in tumor progression and metastasis [51]. The human OVCA cell lines, SKOV3 and SW626, also shared glycoprotein targets with human cell lines of lung (A549 and H460) and blood (K562 and HL60) origins recognized by AvFc. The common AvFc binding partners from these six human cell lines included IGF2R, ITA5, PLXB2, TFR1, and M6PR. Currently the validation of IGF2R as a potential target of AvFc is ongoing. Preliminary immunocytochemistry of SKOV3 cells suggests that AvFc binds regions adjacent to and including IGF2R (Figure 3), suggesting AvFc's ability to recognize IGF2R-associated glycans. While additional experiments are needed to confirm these findings, the presence of multiple *N*-glycosylation sites on the proteins of interest increase the likelihood that high-mannose glycans will occupy these sites and permit recognition by AvFc (Table 3).

Next, we assessed the Fc-mediated function of AvFc utilizing a reporter-cell-based antibody-dependent cell-mediated cytotoxicity (ADCC) assay. Induction of intracellular signaling responsible for ADCC was quantified by luminescence using the FcγRIIIa-expressing Jurkat cell line, which expresses luciferase downstream of FcγRIIIa engagement and activation. Relative to a non-Fc functional lectinbody mutant, AvFc<sup>Agly</sup>, AvFc induced ADCC against all tested OVCA cell lines with an average EC<sub>50</sub> of 6.24 ± 1.97 nM (Figure 2B-D). Taken together, the selective binding and effective induction of ADCC by AvFc justified further investigation of its anticancer activity in an *in vivo* model of OVCA.

To evaluate the *in vivo* efficacy of AvFc, we employed the widely used syngeneic orthotopic ID8-Luciferase (ID8-Luc) OVCA challenge model. In this model, 8-week-old female C57Bl6 mice were intraperitoneally (i.p.) injected with  $2 \times 10^6$  ID8-Luc cells. One week post-challenge, animals were i.p. treated with 15 doses of AvFc (25 mg/kg) or a vehicle control (Figure 4A). Body weight and abdomen circumference of diseased animals began to increase around five weeks post-challenge, indicating the development of ascites (Figure 4C-D). During this period of rapid weight gain on Day 46, bioluminescent imaging was performed and showed a low signal with no significant difference between experimental groups (Figure 4E). A follow-up imaging session a week later produced no signal (data not shown). This poor and inconsistent signal was later attributed to the inconsistent expression of luciferase in the ID8-Luc cells and interference from skin pigmentation and ascites accumulation, leading to the exclusion of this measurement of tumor burden from this experiment [52, 53]. Using survival as the primary endpoint for AvFc's activity in this model, we found that AvFc treatment significantly prolonged median survival from 46 to 63 days (Gehan-Breslow-Wilcoxon test  $p < 0.05$ , Figure 4B).

We then sought to assess the influence of the lectibody on the ID8 tumor immune microenvironment, as these immune cells may interact with AvFc and carry out Fc-mediated effector functions, such as ADCC and ADCP. To establish a baseline understanding of the immune response induced by the syngeneic ID8-Luc cells, mice were challenged with  $3 \times 10^6$  ID8-Luc or a PBS control on Day 0 and treated with a histidine buffer used for AvFc formulation (vehicle) starting from day 7 to 35. At the time of euthanasia, the peritoneal fluid and spleen were collected and analyzed by flow cytometry. We found that the ID8-Luc-challenged mice had a significant presence of natural killer (NK) cells, B cells, dendritic cells, M1-like macrophages, and CD4 T cells in

the peritoneal fluid, in contrast to the significant decrease of these cell types in the spleen (Figure 5). Additionally, M2-like macrophages were significantly increased in the peritoneal lavage of ID8-Luc challenged mice, and the presence of CD8 T cells in the peritoneal fluid was similar to that of the control. Despite the increased infiltration of these immune cells into the peritoneal cavity, the visible presence of tumors at the time of sacrifice confirmed the inability of the immune response to eliminate the tumor.

A subsequent study utilizing the syngeneic ID8-Luc model focused on elucidating the influence of AvFc treatment on the surrounding tumor microenvironment. To assess the immunological impact of AvFc during the treatment course, ID8-challenged mice were treated with AvFc (25 mg/kg) every other day (Q2D) starting on day 7 for a total of 7 doses. Animals were euthanized on day 21, and the peritoneal fluid was utilized for immune cell phenotyping by flow cytometry. AvFc treatment significantly increased the total number of macrophages and classical monocytes in the peritoneal fluid compared to the vehicle control (Figure 6). While AvFc treatment also elevated the number of NK cells, CD8 T cells, and neutrophils, these cell types were not significantly different from those in the vehicle-treated group. These results highlight promising trends in NK cells, M1-like macrophages, and CD8 T cells that may contribute to AvFc's ability to prolong survival in this model. Additionally, hematoxylin and eosin (H&E) staining of ID8-Luc tumors from AvFc-treated animals suggests increased cancer cell death within the tumor, compared to vehicle treated tissues, as indicated by the decreased intensity of hematoxylin staining (Figure 7).

In addition to immunological endpoints of the murine OVCA model, we also examined ID8-Luc tumor tissue (vehicle treated) using fluorescent IHC to observe the pattern of AvFc binding (Figure 8). Using AvFc<sup>Δlec</sup> as a negative control, AvFc was found to decorate the ID8-Luc tumors in a fashion seemingly inverse to the expression of E-

cadherin. Regions bound by AvFc included the outer surface and deeper tumor tissue, which intriguingly showed low E-cadherin expression. In contrast, AvFc did not bind to the medial area of the tumor with high E-cadherin staining. This result provides further support for the activity of AvFc in the ID8-Luc OVCA model, as we have experimentally proven that AvFc binds ID8-Luc-derived tumor tissue. Additionally, this preliminary finding may relate AvFc to the epithelial to mesenchymal transition (EMT) of ID8-Luc cells *in vivo*, as decreased E-cadherin [54] and increased high-mannose glycans [7] are associated with increased progression of OVCA; however, additional experiments are needed to substantiate this claim.

Next, we assessed the translational potential of AvFc by evaluating its ability to recognize human OVCA tissues using IHC, which was performed on a commercial tissue array (US Biomax). Tissues from three stage I high-grade serous ovarian carcinoma patients, aged 48, 72, and 55, and their healthy adjacent tissues were stained with AvFc or AvFc<sup>Δlec</sup> (Figure 9). As demonstrated by the brown DAB staining, AvFc selectively recognized malignant tissues in comparison to the healthy adjacent tissues and the AvFc<sup>Δlec</sup> staining, thus highlighting the increased presence of high-mannose-type glycans in OVCA.



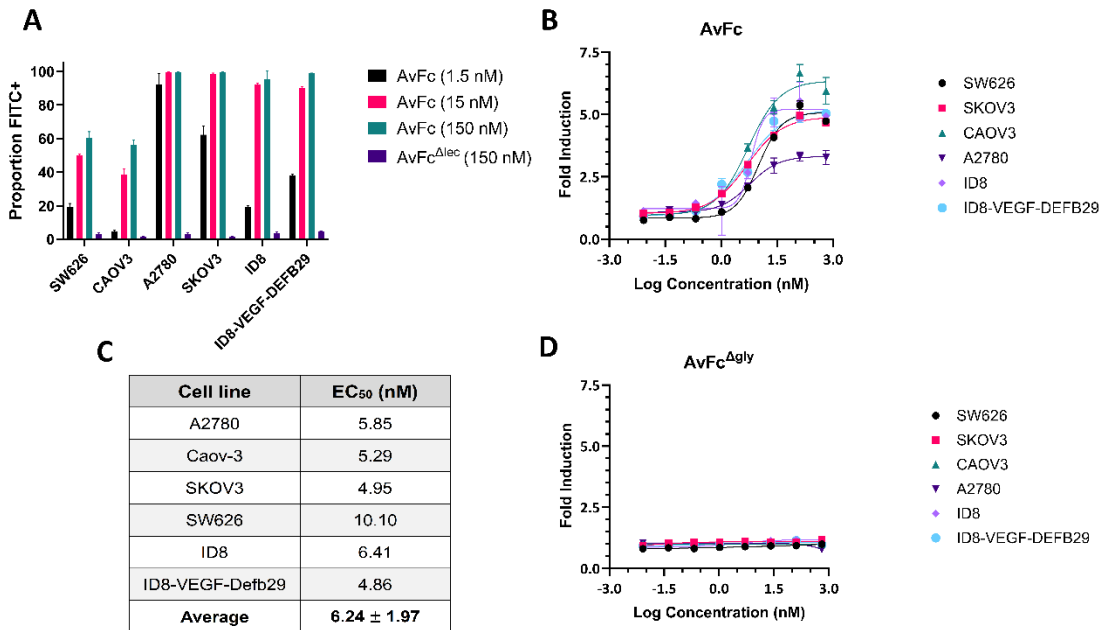


**Figure 2. AvFc binds to and induces ADCC against a panel of OVCA cell lines. (A)**

Flow cytometry assessed AvFc binding to the two murine (ID8, ID8-VEGF-Def2b) and four human (SW626, CAOV3, A2780, and SKOV3) OVCA cell lines. Proportion of FITC+ cells was determined by exclusionary gating of background fluorescence. AvFc demonstrated high binding to most cell lines and achieved saturation at  $\approx 15$  nM, excluding SW626 and CAOV3. AvFc<sup>Δlec</sup> negligibly bound at 150 nM. (B) AvFc induced ADCC in a dose-dependent manner as measured by a reporter cell-based luminescence assay. The average EC<sub>50</sub> of AvFc was  $6.24 \pm 1.97$  nM (C). AvFc<sup>Agly</sup> did not induce ADCC, as expected (D).

	UniProt accession	Gene name	Protein name	Potential N-glycan sites
ID8	P11438	<i>Lamp1</i>	Lysosome-associated membrane glycoprotein 1	19
	Q01279	<i>Egfr</i>	Epidermal growth factor receptor	14
	B2RXS4	<i>Plxnb2</i>	Plexin-B2	14
	P39447	<i>Tjp1</i>	Tight junction protein ZO-1	10
	Q8BZ98	<i>Dnm3</i>	Dynamin-3	5
	Q8R3S6	<i>Exoc1</i>	Exocyst complex component 1	5
	P41731	<i>Cd63</i>	CD63 antigen	4
	P51912	<i>Slc1a5</i>	Neutral amino acid transporter B(0)	2
	P28658	<i>Atxn10</i>	Ataxin-10	1
SKOV3 & SW626	Q92673	<i>SORL1</i>	Sortillin-related receptor	27
	P11717	<i>IGF2R</i>	Cation-independent mannose-6-phosphate receptor	21
	P00533	<i>EGFR</i>	Epidermal growth factor receptor	15
	P08648	<i>ITA5</i>	Integrin alpha-5	14
	O15031	<i>PLXB2</i>	Plexin-B2	14
	P17301	<i>ITGA2</i>	Integrin alpha-2	10
	P02786	<i>TFR1</i>	Transferrin receptor protein 1	5
	P50895	<i>BCAM</i>	Basal cell adhesion molecule	5
	P20645	<i>M6PR</i>	Cation-dependent mannose-6-phosphate receptor	5
Human cell lines	P11717	<i>IGF2R</i>	Cation-independent mannose-6-phosphate receptor	21
	P08648	<i>ITA5</i>	Integrin alpha-5	14
	O15031	<i>PLXB2</i>	Plexin-B2	14
	P02786	<i>TFR1</i>	Transferrin receptor protein 1	5
	P20645	<i>M6PR</i>	Cation-dependent mannose-6-phosphate receptor	5

**Table 3. Potential glycoprotein targets of AvFc.** Co-immunoprecipitation was conducted using AvFc- or AvFc<sup>Δlec</sup>-conjugated agarose resins with cell lysates from various cell lines, including murine OVCA (ID8) and human ovarian (SKOV3, SW626), lung (A549, H460) and blood cancers (K562, HL60). The bound proteins were identified by UHPLC-MS and proteomics analysis to distinguish integral membrane proteins from other cytoplasmic and organelle proteins, in addition to exclusion of proteins identified in the control. The potential N-glycan sites were predicted by NetNGlyc.

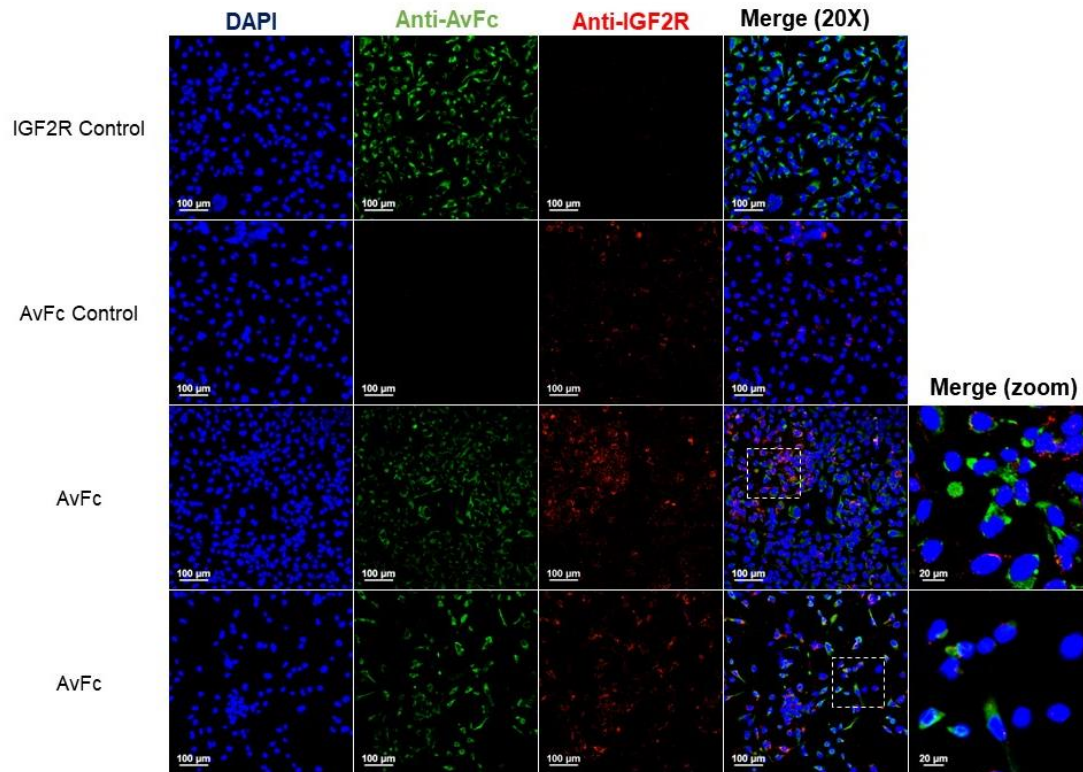


**Figure 3. Preliminary confirmation of IGF2R as a glycoprotein target of AvFc.**

SKOV3 cells were cultured on slides, fixed in methanol, and utilized in immunocytochemistry. Cells were stained with AvFc, anti-IGF2R, and respective fluorophore-conjugated secondary antibodies. The top two rows are secondary antibody only controls for IGF2R and AvFc and show no background fluorescence for the respective channels. The bottom two rows reveal AvFc's broad detection of high-mannose *N*-glycans decorating SKOV3 cells, including regions adjacent to and including IGF2R.

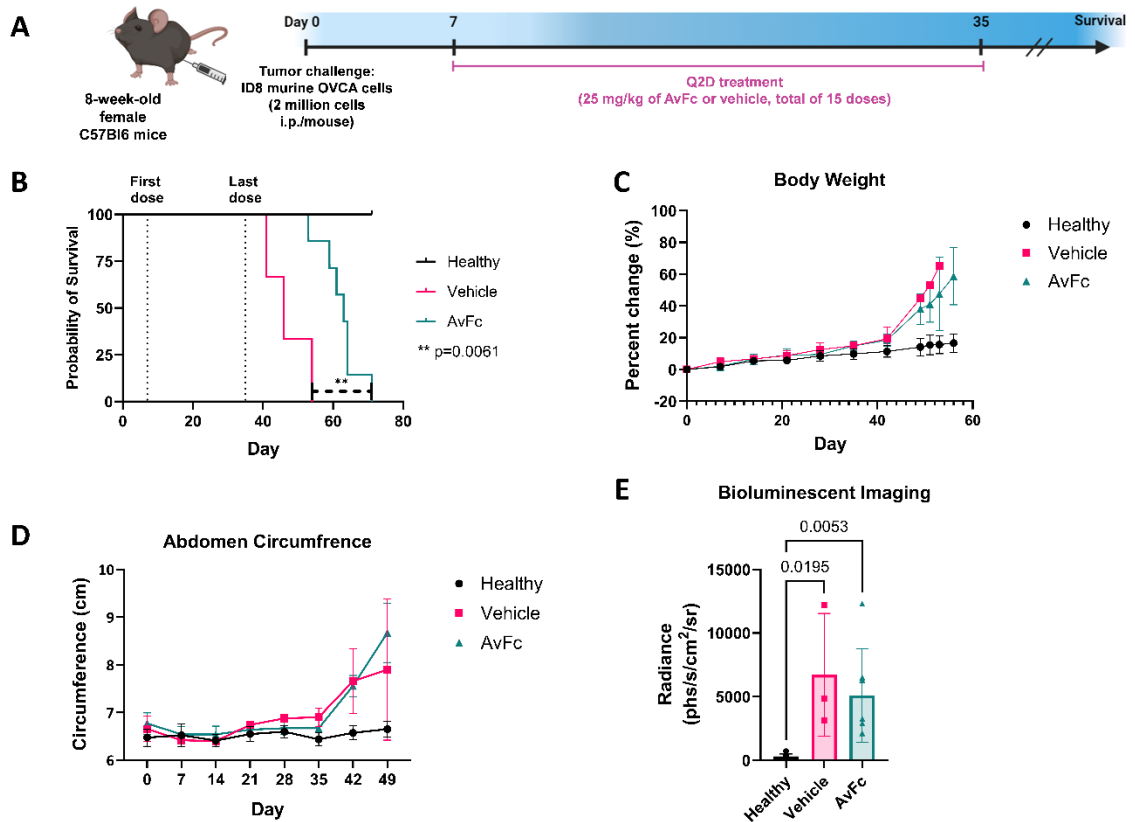
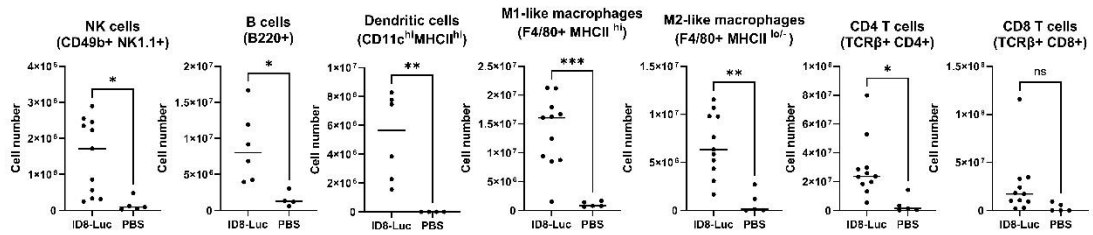


**Figure 4. Effects of AvFc in the ID8-Luc OVCA challenge model.** (A) Eight-week-old female C57Bl6 mice were challenged with  $2 \times 10^6$  ID8-Luc cells on day 0 (n=8 healthy, n=3 vehicle, n=7 AvFc). Treatment with AvFc (25 mg/kg) was initiated on day 7 and continued every other day (Q2D) until day 35 for a total of 15 doses. (B) A Kaplan-Meier curve comparing survival among the experimental groups. AvFc treatment significantly extended survival from a median of 46 to 63 days (\*\* p=0.0061, Gehan-Breslow-Wilcoxon test). (C) Percent change in body weight over the duration of the experiment relative to day 0 weight. Weights of ID8-Luc challenged mice rapidly increased after day 40, with noticeable ascites development around day 42. (D) Abdomen circumference measurements over time showed an increase in size by day 42, consistent with the increase in body weight and ascites development at this time. (E) Bioluminescent

imaging at day 46 did not show a significant difference between groups as quantified by radiance (photons/second/cm<sup>2</sup>/steradian) of the tumor burden *in vivo*.

### Peritoneal lavage



### Spleen

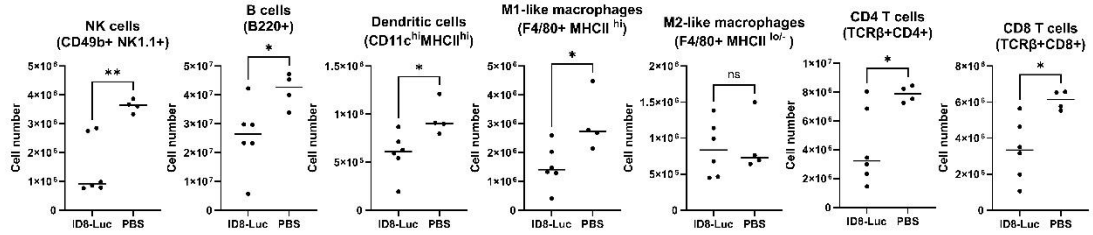


**Figure 5. Immune cell profile of ID8-Luc-challenged animals.** Animals were challenged with  $3 \times 10^6$  ID8-Luc or a PBS control on Day 0 and treated with AvFc formulation buffer (vehicle) starting from day 7 to 35 ( $n=5$  vehicle,  $n=11$  AvFc). After five weeks, animals were euthanized, and immune cells in peritoneal lavage and spleens were analyzed by flow cytometry. Immune cell populations that were significantly elevated in ID8-Luc-challenged animals included natural killer (NK) cells, B cells, dendritic cells, both M1- and M2-like macrophages, and CD4 T cells (\*  $p<0.05$ , \*\*  $p<0.005$ , \*\*\*  $p<0.0005$ , unpaired t-test). These leukocytes were found to be decreased in the spleen to a significant level, excluding M2-like macrophages. Peritoneal lavage CD8 T cells were comparable between groups; however, ID8-Luc animals had significantly lower numbers of CD8 T cells within the spleen.

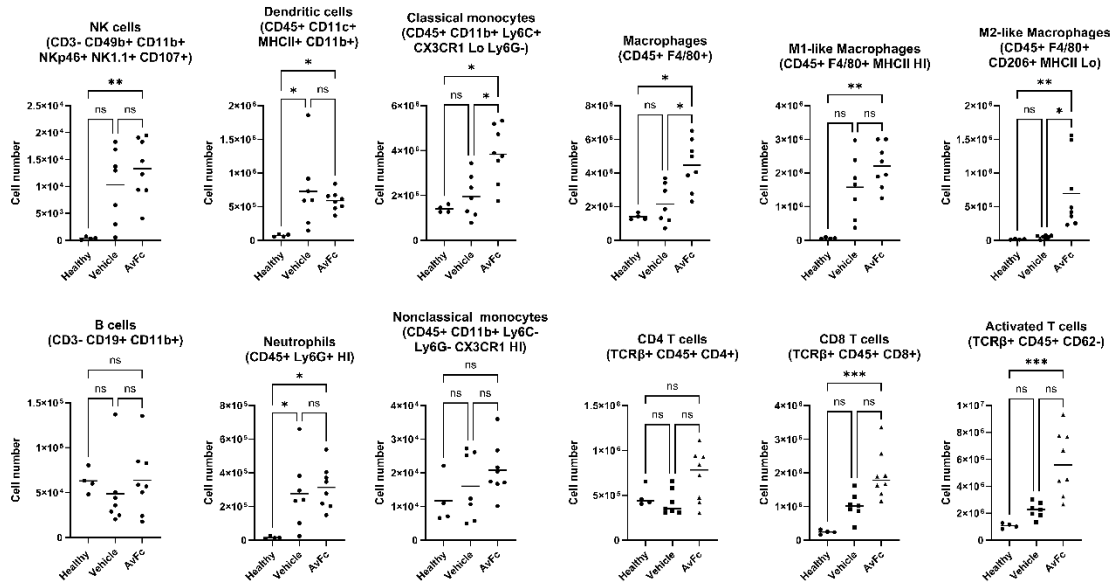


**Figure 6. Immune cell profile of AvFc-treated, ID8-Luc-challenged animals.** Animals

were challenged with  $3 \times 10^6$  ID8-Luc cell line as described (n=4 healthy, n=7 vehicle, n=8 AvFc). Treatment with AvFc (25 mg/kg) was initiated on day 7 and continued every other day for a total of 7 doses. At time of euthanasia, peritoneal lavage was analyzed for immune cells of interest. Classical monocytes, macrophages, and M2-like macrophages were identified to be significantly elevated in the AvFc group as compared to the vehicle control (\* adjusted  $p < 0.05$ , \*\* adjusted  $p < 0.005$ , \*\*\* adjusted  $p < 0.005$ , Kruskal-Wallis test with Dunn's multiple comparisons). Of note, natural killer (NK) cells, M1-like macrophages, neutrophils, non-classical monocytes, CD8 T cells, and activated T cells appear to have a trend of increase but fail to reach significance between the AvFc and vehicle treated groups.

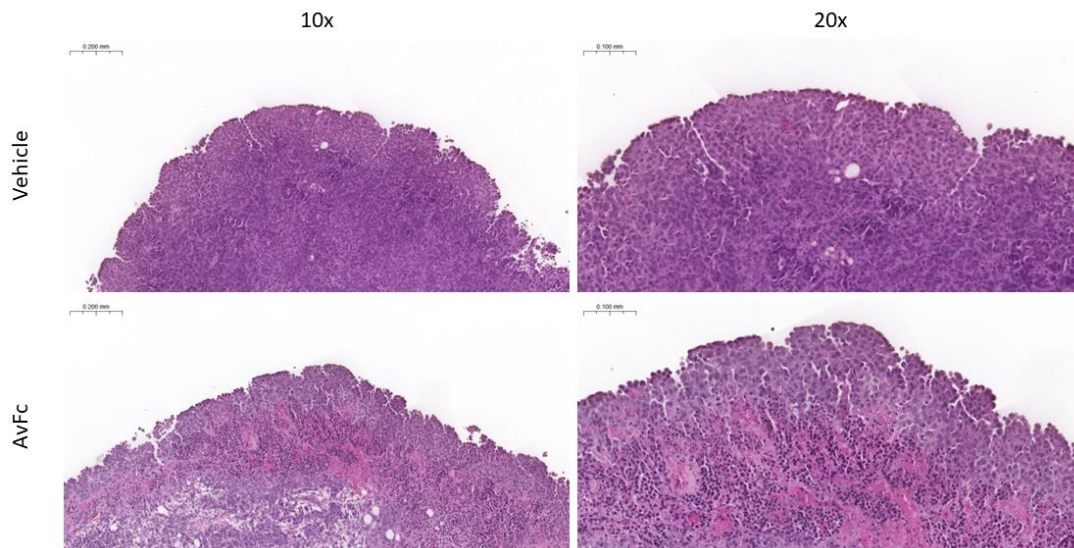


**Figure 7. Representative histology of ID8-Luc-derived tumor tissue.** Tumors from ID8-Luc-challenged mice euthanized on day 21 were formalin-fixed, paraffin embedded, and cut to 10  $\mu$ m thin sections for hematoxylin and eosin (H&E) staining. The vehicle-treated tumor is comprised of an abundance of epithelial cells, as shown by the intensity of hematoxylin (purple) staining of cell nuclei. The AvFc-treated tumor shows a visual increase in eosin (pink) staining, suggesting cancer cell death within the tumor as a result of treatment with 7 doses of AvFc (25 mg/kg).



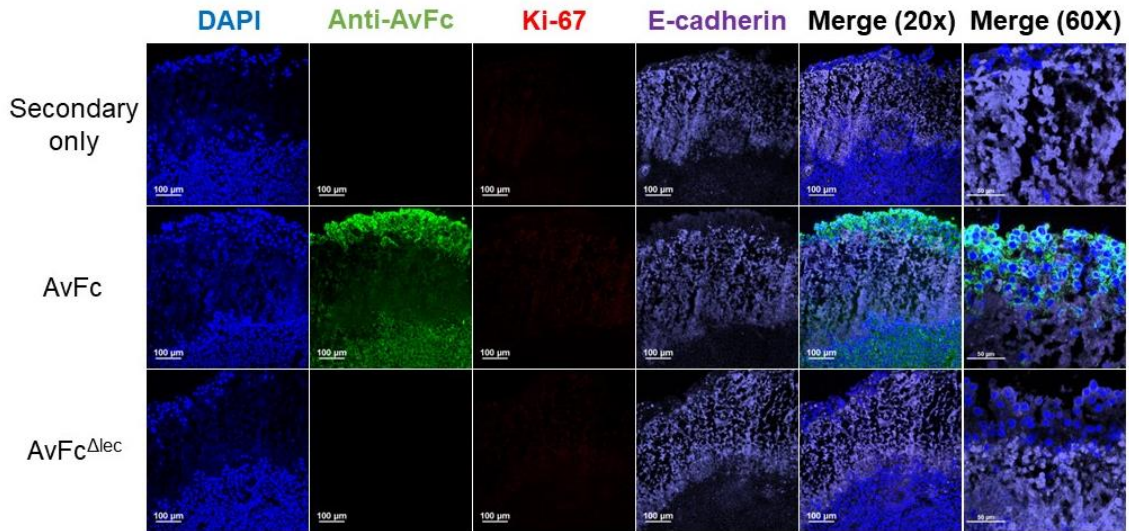


**Figure 8. Fluorescent IHC of AvFc binding to ID8-Luc-derived tumor tissue.** Tumors from ID8-Luc-challenged mice were cryopreserved and cut to 7  $\mu\text{m}$  thin sections for fluorescent immunohistochemistry (IHC). Tissues were stained with AvFc or AvFc <sup>$\Delta\text{lec}$</sup>  and fluorescently labeled anti-human IgG (anti-AvFc), Ki-67, and E-cadherin antibodies. The top row shows the secondary only control, which exhibits no background fluorescence. The middle row displays a vibrant green from the detection of AvFc bound to tumor associated high-mannose glycans, as indicated by the lack of staining from AvFc <sup>$\Delta\text{lec}$</sup>  pictured in the bottom row. AvFc preferentially bound to the external and deep regions of the tumor, with relatively low binding to the middle area of the tumor where high levels of E-cadherin are expressed. Weak Ki-67 signal suggests minimal proliferation of the tumor at this time point.

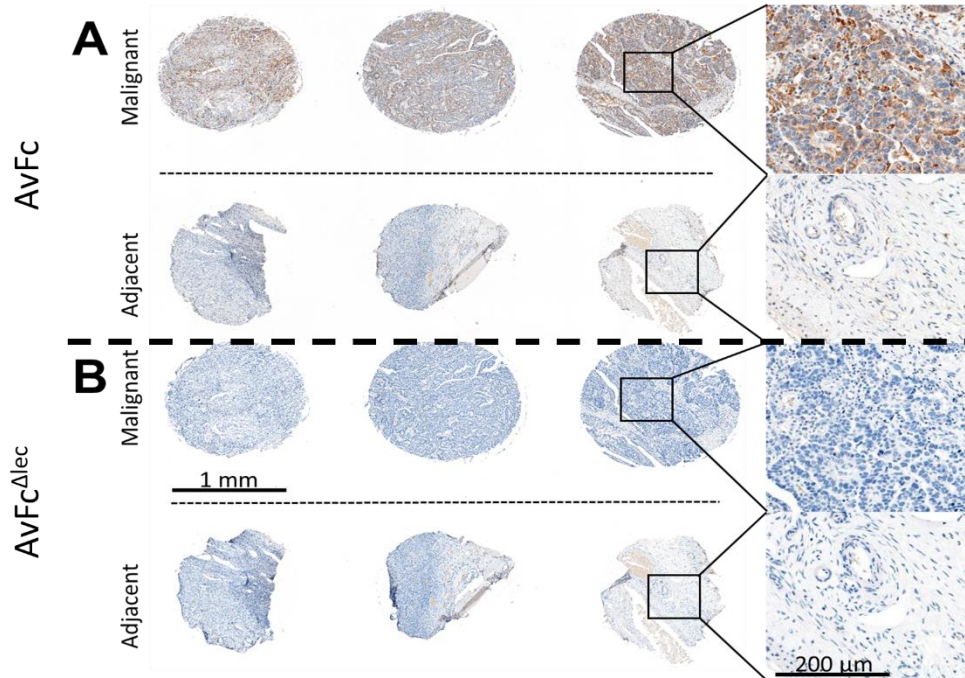


**Figure 9. Conventional IHC of AvFc binding to human OVCA tissues.**

Immunohistochemistry (IHC) was performed on a commercial tissue array by US Biomax (Rockville, MD). In the columns from left to right, tumor tissues were from a 48-year-old, 72-year-old, and a 55-year-old patient. Healthy adjacent tissue was also collected and is pictured below the corresponding malignant tissue. AvFc selectively recognizes human OVCA tissue (A) through the presence of high mannose glycans, as demonstrated by the intensity of DAB staining and lack of binding by AvFc<sup>Δlec</sup> (B).

## CHAPTER 4: DISCUSSION

As more information is discovered about the alteration of the glycome in OVCA, the tumor-associated glycocalyx is stepping into the spotlight as an underappreciated and druggable target. Certain lectins can selectively recognize the abnormal glycan composition induced by the cancerous transformation of normal cells, providing a theoretical basis for further efforts in the development of anticancer lectin therapeutics. To date, however, limited research has been conducted to develop lectins or lectin-based molecules targeting *N*-linked high-mannose glycans overrepresented on the surface of OVCA cells [22, 23, 25]. The work in this thesis provides a solid foundation for further development of AvFc, a lectin-based therapeutic against OVCA.

AvFc is an antibody-like molecule, or “lectibody,” consisting of the recombinant Avaren lectin translationally fused to the Fc region of human IgG1 [42, 46, 47, 50]. In contrast to other lectin molecules, AvFc is neither mitogenic or directly cytotoxic, and it relies on Fc $\gamma$  receptor (Fc $\gamma$ R)-bearing immune cells to orchestrate cancer cell elimination. The experiments shown in this work demonstrate AvFc’s ability to selectively bind to and induce ADCC against human and murine OVCA cell lines (Figure 2A-D). The induction of ADCC likely contributes to the significant extension of survival observed *in vivo* with AvFc treatment in the ID8-Luc challenge model (Figure 4B), and in mouse models of melanoma [47] and lung cancer [50]. Furthermore, an additional mechanism contributing to AvFc’s anticancer activity may include the inhibition of EGFR and IGF1R to prevent cell migration, as described in Oh et. al (2022). Co-immunoprecipitation and proteomics analysis identified EGFR as targets of AvFc in human (SKOV3 and SW626)

and murine (ID8) OVCA cell lines, suggesting that AvFc may also prevent migration through the inhibition of EGFR signaling (Table 3).

Other AvFc targets identified in the proteomic analysis, common between the OVCA cell lines, include PLXB2, a receptor with 14 potential *N*-glycosylation sites (Table 3) and suspected involvement in the proliferation and migration of tumors [51, 55, 56]. Interestingly, PLXB2 serves as a receptor for angiogenin, which contributes to angiogenesis *in vivo* [57]. Studies evaluating PLXB2 in OVCA utilize a micro-RNA, termed miR-126-3p, which downregulates PLXB2 expression and consequently represses OVCA cell proliferation *in vitro* and *in vivo*, supposedly through inhibiting AKT and ERK1/2 signaling pathways [55, 56]. Provided that AvFc binds to the extracellular portion of PLXB2, the lectin body may have an antagonistic effect by blocking angiogenin binding and perhaps impacting downstream signaling pathways, thereby inhibiting tumor growth. However, this hypothesis remains to be experimentally proven.

Other common targets of AvFc from the human cell lines included IGF2R, ITA5, TFR1, and M6PR. These glycoproteins, all containing multiple potential *N*-glycosylation sites (Table 3), function as receptors, adhesion molecules, or transporters and exist as dimers on the cell surface, thus increasing the density of *N*-glycans within a small area. The confirmation of IGF2R as a target of AvFc is in progress, with preliminary immunocytochemistry data suggesting AvFc's recognition of IGF2R associated and adjacent high-mannose glycans on SKOV3 cells (Figure 3). In OVCA, IGF2R function is lost by cancer-related mutations (loss of heterozygosity) therefore preventing IGF2R from sequestering its ligand, insulin growth factor 2, and allowing it to bind alternate receptors and promote metastasis and immunosuppression [58-61]. Additional experiments are needed to confirm AvFc's interactions with these proteins and their

biological implications; however, the numerous *N*-glycosylation sites on these proteins increases the potential of AvFc binding (Table 3).

The present study also demonstrated the *in vivo* activity of AvFc in the syngeneic orthotopic ID8-Luc OVCA challenge model where 15 doses of AvFc (25 mg/kg) significantly extended median survival from 46 to 63 days compared to the vehicle control (Figure 4B). Measurements of body weight and abdomen circumference during this study did not accurately reflect the health of the animal, as many animals became moribund before reaching the humane endpoints (35 g and/or 10 cm, Figure 4C-D). This may be related to the development of ascites, or the accumulation of fluid in the peritoneum that includes metastatic cancer cells, immune cells, cytokines, and blood among other components [62, 63]. An individual mouse may develop up to 15 mL of ascites, however even small amounts of this fluid might impact the health of the animal, resulting in a moribund state before reaching the humane endpoints. The development of ascites may also explain the inconsistent signal measured during bioluminescent imaging (Figure 4E), as the injected luciferin could have been diluted to an usable level [52]. Additionally, the use of C57Bl6 mice with dark pigmented fur, without hair removal, may have resulted in the attenuation of bioluminescent signal [53]. Upon *in vitro* evaluation of the ID8-Luc cells, luminescence was identified to be varied across cell passages, suggesting the heterogenous retention of luciferase expression (data not shown). Future experiments will be designed to improve the bioluminescent signal *in vivo* through the recovery of luciferase expression in ID8-Luc cells and removal of abdominal hair prior to imaging.

Given that AvFc's efficacy critically depends on the nature of antitumor immunity naturally induced against the tumor, it was imperative to characterize the baseline immune cell profile of the ID8-Luc challenge model. A previous report by Liao et al. has

demonstrated that the expression of the xenogeneic antigen, firefly luciferase, in the ID8-Luc cell line did not alter the intraperitoneal tumor immune microenvironment in comparison to the non-luciferase expressing original cell line, underscoring the appropriateness of this model for immunological investigations of OVCA [63]. The syngeneic ID8-Luc model revealed a significant presence of NK cells, B cells, dendritic cells, M1-like macrophages, and CD4 T cells in the peritoneal fluid, all of which were found to be depleted in the spleen (Figure 5). The elevation of B cells, CD4 T cells, and dendritic cells compare to the immune cell phenotype generated by green fluorescent protein expressing ID8 cells *in vivo* [64]. Although, the ID8-Luc model behaved more similar to a wild type ID8 cell line with similar patterns of increase for all significant cell types in the peritoneal fluid, excluding NK cells which were not measured in the *in vivo* evaluation of wild type ID8 cells [65]. As the syngeneic ID8-Luc cells were injected i.p., the accumulation of immune cells into the peritoneal cavity was expected. The reduced leukocyte populations of the spleen, the secondary lymphoid organ draining the peritoneal cavity, suggest that the immune cells may have been redirected toward the site of inflammation within the peritoneum or migrated to other lymph nodes. However, the presence of these peritoneal leukocytes was insufficient to eradicate the cancer since tumor nodules were still present at time of sacrifice, providing implications for immunotherapeutic strategies.

A major finding of the present study was the impact of 7 doses of AvFc (25 mg/kg) on the ID8-Luc immune microenvironment (Figure 6). In comparison to the disease control, AvFc treatment significantly increased the number of FcγR-bearing cells, particularly macrophages, which express all classes of FcγRs and may contribute to cancer cell elimination through ADCP [66]. NK cells, which primarily express FcγRIIIa, are likely activated by AvFc to exert ADCC, as suggested by *in vitro* ADCC assays

(Figure 1, 2) and previous *in vivo* models of lung cancer in SCID mice, which are deficient in B and T cells and retain NK cells, macrophages, and granulocytes [47, 50]. Though NK cells in the AvFc group were not statistically different from the vehicle control, there was a trend of increase that may prove to become significant with additional doses of AvFc. This snapshot of the immune landscape early during AvFc treatment also demonstrates an increase in peritoneal leukocytes, possibly indicating a move toward an improved antitumor immune response comprised of M1-like macrophages, NK cells, activated T cells, and CD8 T cells for effective elimination of the tumor [40, 67]. Interestingly, M2-like macrophages were significantly elevated in the AvFc group in comparison to the disease control. Still, AvFc treatment significantly elevated total macrophages and retains a ratio of M1/M2-like cells comparable to the healthy control (data not shown). However, this observation of increased M2-like macrophages may be attributed to the apoptosis of cancer cells at this timepoint [68]. The evaluation of M2-like macrophages after prolonged treatment with AvFc will provide a better understanding of the balance of pro- vs antitumor immunity in this model.

Both classical and nonclassical monocytes also appeared to be elevated during AvFc treatment, albeit to different levels relative to vehicle, which may also act as pro-tumor mediators. However, there is contrasting evidence supporting their antitumor activity, depending on the composition of the tumor microenvironment [69, 70]. Research conducted by Dent, et al. (2022) identified a significant presence of nonclassical monocytes within B16F10 murine melanoma tumors, which was associated with significant reduction in tumor volume following AvFc treatment. This indicates the significant contribution of these cells to the lectinibody's antitumor effects. Evaluation of cytokine levels (e.g., IL-10, TGF $\beta$ , IFN $\gamma$ , and TNF $\alpha$ ) in the peritoneal fluid would assist in

elucidating the function of these cell types in response to AvFc treatment in the ID8-Luc model [40, 69].

The results presented here describing the increase of leukocytes in the peritoneal fluid of AvFc-treated, ID8-challenged animals present a unique immune composition in comparison to other conventional intraperitoneal treatments evaluated in this model. Investigations into the immune response following a single dose of various standard chemotherapeutic agents and select combinations identified the dual treatment of carboplatin and paclitaxel as the least immunosuppressive, demonstrated by a decrease in CD4, CD8, and regulatory T cells, macrophages, monocytes relative to the disease control [71]. Also, multiple doses of cisplatin have been found to elevate Ly6C<sup>+</sup> monocytes (including classical monocytes) while decreasing CD8 T cells and naïve T cells [72]. Additionally, an ID8 model overexpressing VEGF was used to evaluate the influence of IL-12 administration with and without dual immune checkpoint inhibitor treatment (anti-PD1 and anti-CTLA4) and resulted in a significant decrease in macrophages and dendritic cells in both scenarios, while CD8 T cell numbers remained similar to the control [73]. Unlike the other intraperitoneal administered chemotherapeutics and immune checkpoint inhibitors, AvFc works to achieve an active immune environment where the significant increase in macrophages likely plays a role in ADCP and processing free tumor antigens potentially released as a result of NK cell mediated ADCC. Though 7 doses of AvFc only appears to have a trend of increase for NK cells, the expression of CD107a is known to be associated with cytotoxic activity, supporting this hypothesis [74]. Limited information is available on the ID8 model regarding the immunological validation of ADCC or ADCP *in vivo*, however depletion of NK cells and macrophages may elucidate the role of these cytotoxic mechanisms in AvFc's antitumor efficacy. One particular study that tested the antitumor activity of an



anti-CD47 monoclonal antibody with ADCC and ADCP-activating murine IgG2b subclass, expressed by an oncolytic herpesvirus, demonstrated significantly extended survival compared to the same antibody with a murine IgG3 subclass, a poor inducer of ADCC and ADCP, *in vivo* in ID8-challenged mice. Furthermore, the efficacy of the IgG2b version of the anti-CD47 antibody was significantly compromised by the depletion of NK cells and macrophages (in separate experiments), suggesting the potential contribution of ADCC and ADCP to antitumor activity in this model [75]. Other mouse models may also be employed to assess ADCC *in vivo*, such a novel immunodeficient NOG-FcγR-deficient human IL-15 transgenic mouse strain that lacks FcγRs and mouse innate cell-mediated ADCC and is thus suitable for the evaluation of ADCC carried out by transplanted human NK cells [76]. However, more available immunodeficient mouse strains like NOD/SCID and NOD/SCID Il2rg<sup>null</sup> mice may also be utilized to demonstrate ADCC *in vivo*, with proper controls, as NK cells are dysfunctional or nonexistent in these animals [77]. Future experiments designed to determine the involvement of ADCC and ADCP in AvFc's antitumor activity will need to utilize immunodeficient mice to understand the contributions of the immune system in AvFc's *in vivo* efficacy.

A limitation of the current study is the examination of immune cells solely in the peritoneal fluid and not those within the tumor, the latter of which holds major prognostic and predictive importance for OVCA [41]. Future studies will aim to assess the immune composition of ID8-Luc tumors. Nevertheless, H&E staining of tumors from AvFc-treated animals suggests an increase of intratumoral cancer cell death relative to the vehicle control. This observation aligns with the significantly extended overall survival of these animals, setting a promising precedence for the identification of immune cells within the tumor (Figure 7).

Fluorescent IHC was used to confirm AvFc binding to ID8-Luc-derived tumor tissue, but in doing so, we identified an interesting binding pattern of AvFc that is inversely related to the expression of E-cadherin (Figure 8). This preliminary data may suggest a link between the EMT of malignant cells [54] and the observed increase of high-mannose glycans [7] and dysregulated glycosylation machinery in OVCA [6]. A study evaluating metastasis in cholangiocarcinoma demonstrated, both *in vitro* and *in vivo*, that increased cell-surface high-mannose glycans results in a higher metastatic potential of cholangiocarcinoma cells [10]. Limited studies in OVCA have experimentally investigated this relationship between glycosylation and metastasis. However, the *Rhizoctonia bataticola* lectin, has been shown to bind and inhibit SKOV3 and OVCAR3 OVCA cell migration *in vitro* [23, 24]. Previous work on AvFc has demonstrated the importance of glycan binding in inhibiting A549 and H460 lung cancer cell migration *in vitro* and reducing *in vivo* tumor burden in metastasis models of A549 lung cancer and B16F10 murine melanoma, although these findings have yet to be explored in OVCA models [47, 50]. Thus, there is evidence that lectins and lectin-based molecules, like AvFc, may be able to effectively target metastatic cancer cells.

When developing new anticancer biologics for human application, it is of utmost importance to assess their selectivity toward the intended malignancy. To address this concern in the present study, IHC was performed and revealed AvFc's selective, high-mannose-glycan-based recognition of stage I high-grade serous OVCA tissues over matched healthy adjacent tissue (Figure 9). This pattern has also been observed in primary NSCLC tissues reported in Oh et. al (2022), with additional evidence proving effective *in vitro* induction of ADCC using human PBMCs. Though, future studies should evaluate AvFc's selectivity toward a variety of stages and types of OVCA to assess its utility for clinical studies and translation.

In conclusion, the present study has investigated the anti-OVCA activity of AvFc, a lectin body selective toward cancer-associated *N*-linked high-mannose glycans. Findings of major importance for the development of AvFc as a therapeutic against OVCA include the prolonged survival and increased recruitment of FcγR-bearing immune cells in the syngeneic ID8-Luc OVCA challenge model, as well as the selective recognition of patient-derived OVCA tumors. Furthermore, AvFc was shown to target *N*-glycan-rich glycoproteins that function as receptors, transporters, and adhesion molecules, as well as murine OVCA tumor tissues with low E-cadherin expression. Taken together, these results highlight OVCA-associated high-mannose glycans as a druggable target that AvFc effectively leverages to induce cancer cell elimination.

## REFERENCES

1. Stanley, P., Taniguchi, N., and Aebi, M., *Essentials of Glycobiology [Internet]*. . 3 ed. Vol. Chapter 9. 2017, Cold Spring Harbor (NY): Cold Spring Harbor Laboratory Press.
2. Stowell, S.R., T. Ju, and R.D. Cummings, *Protein glycosylation in cancer*. *Annu Rev Pathol*, 2015. **10**: p. 473-510.
3. Thomas, D., A.K. Rathinavel, and P. Radhakrishnan, *Altered glycosylation in cancer: A promising target for biomarkers and therapeutics*. *Biochim Biophys Acta Rev Cancer*, 2021. **1875**(1): p. 188464.
4. Pucci, M., N. Malagolini, and F. Dall'Olio, *Glycobiology of the Epithelial to Mesenchymal Transition*. *Biomedicines*, 2021. **9**(7).
5. Pinho, S.S., et al., *Loss and Recovery of Mgat3 and GnT-III Mediated E-cadherin N-glycosylation Is a Mechanism Involved in Epithelial-Mesenchymal-Epithelial Transitions*. *PLOS ONE*, 2012. **7**(3): p. e33191.
6. Hu, Y., et al., *Integrated Proteomic and Glycoproteomic Characterization of Human High-Grade Serous Ovarian Carcinoma*. *Cell Reports*, 2020. **33**(3).
7. Chen, H., et al., *Mass spectrometric profiling reveals association of N-glycan patterns with epithelial ovarian cancer progression*. *Tumour Biol*, 2017. **39**(7): p. 1010428317716249.
8. Ruhaak, L.R., et al., *Differential N-Glycosylation Patterns in Lung Adenocarcinoma Tissue*. *J Proteome Res*, 2015. **14**(11): p. 4538-49.
9. Möglinger, U., et al., *Alterations of the Human Skin N- and O-Glycome in Basal Cell Carcinoma and Squamous Cell Carcinoma*. *Front Oncol*, 2018. **8**: p. 70.
10. Park, D.D., et al., *Metastasis of cholangiocarcinoma is promoted by extended high-mannose glycans*. *Proceedings of the National Academy of Sciences*, 2020. **117**(14): p. 7633-7644.
11. de Leoz, M.L., et al., *High-mannose glycans are elevated during breast cancer progression*. *Mol Cell Proteomics*, 2011. **10**(1): p. M110.002717.
12. Park, H.M., et al., *Mass spectrometry-based N-linked glycomic profiling as a means for tracking pancreatic cancer metastasis*. *Carbohydr Res*, 2015. **413**: p. 5-11.
13. Sethi, M.K., W.S. Hancock, and S. Fanayan, *Identifying N-Glycan Biomarkers in Colorectal Cancer by Mass Spectrometry*. *Acc Chem Res*, 2016. **49**(10): p. 2099-2106.
14. Dan, X., W. Liu, and T.B. Ng, *Development and Applications of Lectins as Biological Tools in Biomedical Research*. *Med Res Rev*, 2016. **36**(2): p. 221-47.
15. Fu, L.L., et al., *Plant lectins: targeting programmed cell death pathways as antitumor agents*. *Int J Biochem Cell Biol*, 2011. **43**(10): p. 1442-9.
16. Mazalovska, M. and J.C. Kouokam, *Plant-Derived Lectins as Potential Cancer Therapeutics and Diagnostic Tools*. *Biomed Res Int*, 2020. **2020**: p. 1631394.
17. Yau, T., et al., *Lectins with potential for anti-cancer therapy*. *Molecules*, 2015. **20**(3): p. 3791-810.
18. Liu, B., M.W. Min, and J.K. Bao, *Induction of apoptosis by Concanavalin A and its molecular mechanisms in cancer cells*. *Autophagy*, 2009. **5**(3): p. 432-3.

19. Roy, B., et al., *Role of PI3K/Akt/mTOR and MEK/ERK pathway in Concanavalin A induced autophagy in HeLa cells*. Chem Biol Interact, 2014. **210**: p. 96-102.
20. Miyagi, T., et al., *Concanavalin a injection activates intrahepatic innate immune cells to provoke an antitumor effect in murine liver*. Hepatology, 2004. **40**(5): p. 1190-6.
21. Chang, C.P., et al., *Concanavalin A induces autophagy in hepatoma cells and has a therapeutic effect in a murine in situ hepatoma model*. Hepatology, 2007. **45**(2): p. 286-96.
22. Gondim, A.C.S., et al., *The potent anti-cancer activity of Dioclea lasiocarpa lectin*. J Inorg Biochem, 2017. **175**: p. 179-189.
23. Hegde, P., et al., *Rhizoctonia bataticola lectin induces apoptosis and inhibits metastasis in ovarian cancer cells by interacting with CA 125 antigen differentially expressed on ovarian cells*. Glycoconj J, 2021. **38**(6): p. 669-688.
24. Nagre, N.N., et al., *A potent mitogenic lectin from the mycelia of a phytopathogenic fungus, Rhizoctonia bataticola, with complex sugar specificity and cytotoxic effect on human ovarian cancer cells*. Glycoconj J, 2010. **27**(3): p. 375-86.
25. Schumacher, U., S. Feldhaus, and U. Mengs, *Recombinant mistletoe lectin (rML) is successful in treating human ovarian cancer cells transplanted into severe combined immunodeficient (SCID) mice*. Cancer Letters, 2000. **150**(2): p. 171-175.
26. Zwierzina, H., et al., *The preclinical and clinical activity of aviscumine: a potential anticancer drug*. Eur J Cancer, 2011. **47**(10): p. 1450-7.
27. Siegel, R.L., A.N. Giaquinto, and A. Jemal, *Cancer statistics, 2024*. CA Cancer J Clin, 2024. **74**(1): p. 12-49.
28. Devouassoux-Shisheboran, M. and C. Genestie, *Pathobiology of ovarian carcinomas*. Chin J Cancer, 2015. **34**(1): p. 50-5.
29. Matulonis, U.A., et al., *Ovarian cancer*. Nature Reviews Disease Primers, 2016. **2**(1): p. 16061.
30. Prat, J., *New insights into ovarian cancer pathology*. Annals of Oncology, 2012. **23**: p. x111-x117.
31. Lheureux, S., et al., *Epithelial ovarian cancer*. The Lancet, 2019. **393**(10177): p. 1240-1253.
32. Berek, J.S., et al., *Cancer of the ovary, fallopian tube, and peritoneum: 2021 update*. International Journal of Gynecology & Obstetrics, 2021. **155**(S1): p. 61-85.
33. Zhang, M., et al., *Roles of CA125 in diagnosis, prediction, and oncogenesis of ovarian cancer*. Biochim Biophys Acta Rev Cancer, 2021. **1875**(2): p. 188503.
34. Veneziani, A.C., et al., *Heterogeneity and treatment landscape of ovarian carcinoma*. Nat Rev Clin Oncol, 2023. **20**(12): p. 820-842.
35. Richardson, D.L., R.N. Eskander, and D.M. O'Malley, *Advances in Ovarian Cancer Care and Unmet Treatment Needs for Patients With Platinum Resistance: A Narrative Review*. JAMA Oncol, 2023. **9**(6): p. 851-859.
36. Luu, A.Z., et al., *Role of Endothelium in Doxorubicin-Induced Cardiomyopathy*. JACC Basic Transl Sci, 2018. **3**(6): p. 861-870.
37. Gordon, A.N., et al., *Recurrent epithelial ovarian carcinoma: a randomized phase III study of pegylated liposomal doxorubicin versus topotecan*. J Clin Oncol, 2001. **19**(14): p. 3312-22.
38. Indini, A., et al., *Immune-Checkpoint Inhibitors in Platinum-Resistant Ovarian Cancer*. Cancers (Basel), 2021. **13**(7).

39. Barber, E. and D. Matei, *Immunotherapy in ovarian cancer: we are not there yet*. *Lancet Oncol*, 2021. **22**(7): p. 903-905.
40. Martinez, A., et al., *Preclinical and Clinical Immunotherapeutic Strategies in Epithelial Ovarian Cancer*. *Cancers (Basel)*, 2020. **12**(7).
41. Fanale, D., et al., *Prognostic and Predictive Role of Tumor-Infiltrating Lymphocytes (TILs) in Ovarian Cancer*. *Cancers (Basel)*, 2022. **14**(18).
42. Hamorsky, K.T., et al., *Engineering of a Lectibody Targeting High-Mannose-Type Glycans of the HIV Envelope*. *Molecular Therapy*, 2019. **27**(11): p. 2038-2052.
43. Suzuki, K., et al., *Peculiarity in crystal packing of anti-HIV lectin actinohivin in complex with  $\alpha(1-2)$ mannobiose*. *Acta Crystallogr D Biol Crystallogr*, 2013. **69**(Pt 9): p. 1818-25.
44. Zhang, F., et al., *The characteristic structure of anti-HIV actinohivin in complex with three HMTG D1 chains of HIV-gp120*. *Chembiochem*, 2014. **15**(18): p. 2766-73.
45. Matoba, N., et al., *HIV-1 neutralization profile and plant-based recombinant expression of actinohivin, an Env glycan-specific lectin devoid of T-cell mitogenic activity*. *PLoS One*, 2010. **5**(6): p. e111443.
46. Dent, M., et al., *Safety and Efficacy of Avaren-Fc Lectibody Targeting HCV High-Mannose Glycans in a Human Liver Chimeric Mouse Model*. *Cellular and Molecular Gastroenterology and Hepatology*, 2021. **11**(1): p. 185-198.
47. Dent, M., et al., *Impact of glycoengineering and antidrug antibodies on the anticancer activity of a plant-made lectin-Fc fusion protein*. *Plant Biotechnol J*, 2022. **20**(11): p. 2217-2230.
48. Seber Kasinger, L.E., et al., *A novel anti-HIV-1 bispecific bNAb-lectin fusion protein engineered in a plant-based transient expression system*. *Plant Biotechnol J*, 2019. **17**(8): p. 1646-1656.
49. Strasser, R., et al., *Generation of glyco-engineered *Nicotiana benthamiana* for the production of monoclonal antibodies with a homogeneous human-like N-glycan structure*. *Plant Biotechnol J*, 2008. **6**(4): p. 392-402.
50. Oh, Y.J., et al., *Antitumor activity of a lectibody targeting cancer-associated high-mannose glycans*. *Mol Ther*, 2022. **30**(4): p. 1523-1535.
51. Toledano, S. and G. Neufeld, *Plexins as Regulators of Cancer Cell Proliferation, Migration, and Invasivity*. *Cancers (Basel)*, 2023. **15**(16).
52. Baert, T., et al., *The dark side of ID8-Luc2: pitfalls for luciferase tagged murine models for ovarian cancer*. *J Immunother Cancer*, 2015. **3**: p. 57.
53. Curtis, A., et al., *Temporal variations of skin pigmentation in C57BL/6 mice affect optical bioluminescence quantitation*. *Mol Imaging Biol*, 2011. **13**(6): p. 1114-23.
54. Kielbik, M., I. Szulc-Kielbik, and M. Klink, *E-Cadherin Expression in Relation to Clinicopathological Parameters and Survival of Patients with Epithelial Ovarian Cancer*. *Int J Mol Sci*, 2022. **23**(22).
55. Xiang, G. and Y. Cheng, *MiR-126-3p inhibits ovarian cancer proliferation and invasion via targeting PLXNB2*. *Reprod Biol*, 2018. **18**(3): p. 218-224.
56. Liang, Y., K. Meng, and R. Qiu, *Circular RNA *Circ\_0013958* Functions as a Tumor Promoter in Ovarian Cancer by Regulating miR-637/PLXNB2 Axis*. *Front Genet*, 2021. **12**: p. 644451.
57. Yu, W., et al., *Plexin-B2 Mediates Physiologic and Pathologic Functions of Angiogenin*. *Cell*, 2017. **171**(4): p. 849-864.e25.
58. Liefers-Visser, J.A.L., et al., *IGF system targeted therapy: Therapeutic opportunities for ovarian cancer*. *Cancer Treat Rev*, 2017. **60**: p. 90-99.
59. Belfiore, A., et al., *IGF2: A Role in Metastasis and Tumor Evasion from Immune Surveillance?* *Biomedicines*, 2023. **11**(1).

60. Kuhlmann, J.D., et al., *Loss of heterozygosity proximal to the M6P/IGF2R locus is predictive for the presence of disseminated tumor cells in the bone marrow of ovarian cancer patients before and after chemotherapy*. Genes Chromosomes Cancer, 2011. **50**(8): p. 598-605.
61. Martin-Kleiner, I. and K. Gall Troselj, *Mannose-6-phosphate/insulin-like growth factor 2 receptor (M6P/IGF2R) in carcinogenesis*. Cancer Lett, 2010. **289**(1): p. 11-22.
62. Rickard, B.P., et al., *Malignant Ascites in Ovarian Cancer: Cellular, Acellular, and Biophysical Determinants of Molecular Characteristics and Therapy Response*. Cancers, 2021. **13**(17): p. 4318.
63. Liao, J.B., et al., *Preservation of tumor-host immune interactions with luciferase-tagged imaging in a murine model of ovarian cancer*. J Immunother Cancer, 2015. **3**: p. 16.
64. Pisano, S., et al., *Assessment of the immune landscapes of advanced ovarian cancer in an optimized in vivo model*. Clinical and Translational Medicine, 2021. **11**(10): p. e551.
65. Rodriguez, G.M., et al., *The Tumor Immune Profile of Murine Ovarian Cancer Models: An Essential Tool For Ovarian Cancer Immunotherapy Research*. Cancer Res Commun, 2022. **2**(6): p. 417-433.
66. Weiskopf, K. and I.L. Weissman, *Macrophages are critical effectors of antibody therapies for cancer*. MAbs, 2015. **7**(2): p. 303-10.
67. Yang, S., et al., *The shedding of CD62L (L-selectin) regulates the acquisition of lytic activity in human tumor reactive T lymphocytes*. PLoS One, 2011. **6**(7): p. e22560.
68. Zhang, Q., et al., *Apoptotic SKOV3 cells stimulate M0 macrophages to differentiate into M2 macrophages and promote the proliferation and migration of ovarian cancer cells by activating the ERK signaling pathway*. Int J Mol Med, 2020. **45**(1): p. 10-22.
69. Jeong, J., Y. Suh, and K. Jung, *Context Drives Diversification of Monocytes and Neutrophils in Orchestrating the Tumor Microenvironment*. Front Immunol, 2019. **10**: p. 1817.
70. Olingy, C.E., H.Q. Dinh, and C.C. Hedrick, *Monocyte heterogeneity and functions in cancer*. J Leukoc Biol, 2019. **106**(2): p. 309-322.
71. Vankerckhoven, A., et al., *Type of chemotherapy has substantial effects on the immune system in ovarian cancer*. Transl Oncol, 2021. **14**(6): p. 101076.
72. Hopkins, D., et al., *Cisplatin increases immune activity of monocytes and cytotoxic T-cells in a murine model of epithelial ovarian cancer*. Transl Oncol, 2021. **14**(12): p. 101217.
73. Pavicic, P.G., Jr., et al., *Immunotherapy with IL12 and PD1/CTLA4 inhibition is effective in advanced ovarian cancer and associates with reversal of myeloid cell-induced immunosuppression*. Oncoimmunology, 2023. **12**(1): p. 2198185.
74. Aktas, E., et al., *Relationship between CD107a expression and cytotoxic activity*. Cell Immunol, 2009. **254**(2): p. 149-54.
75. Tian, L., et al., *Targeting Fc Receptor-Mediated Effects and the "Don't Eat Me" Signal with an Oncolytic Virus Expressing an Anti-CD47 Antibody to Treat Metastatic Ovarian Cancer*. Clinical Cancer Research, 2022. **28**(1): p. 201-214.
76. Katano, I., et al., *Improved Detection of in vivo Human NK Cell-Mediated Antibody-Dependent Cellular Cytotoxicity Using a Novel NOG-FcyR-Deficient Human IL-15 Transgenic Mouse*. Frontiers in Immunology, 2020. **11**.

77. Chen, J., et al., *The development and improvement of immunodeficient mice and humanized immune system mouse models*. Front Immunol, 2022. **13**: p. 1007579.



## CURRICULUM VITAE

NAME: Katarina Lee Mayer  
ADDRESS: Clinical and Translational Research Building  
505 South Hancock Street Lab 442  
Louisville, Kentucky 40202

### EDUCATION:

M.S. Pharmacology & Toxicology	University of Louisville	Currently enrolled
B.S. Biology	University of Louisville	2018-2021
Honors Thesis: "Relations between maternal language input and child language development for children with Williams syndrome." (PI: Dr. Carolyn B. Mervis)		
Degree Honors: Magna cum laude		
A.S.	Owensboro Community and Technical College	2016-2018
Degree Honors: With High Distinction		
A.A.	Owensboro Community and Technical College	2016-2018
Degree Honors: With High Distinction		

### AWARDS:

Integrated Programs in Biomedical Sciences Fellowship	2022-present
1 <sup>st</sup> Place Poster Award, Master's Basic Science Graduate Student Category at Research! Louisville	2023
National Cancer Institute R25 Cancer Education Program	2021

### PUBLICATION:

Dent, M., **Mayer, K. L.**, Verjan Garcia, N., Guo, H., Kajiura, H., Fujiyama, K., & Matoba, N. (2022). Impact of glycoengineering and antidrug antibodies on the anticancer activity of a plant-made lectin-Fc fusion protein. *Plant Biotechnol J*, 20(11), 2217-2230. doi:10.1111/pbi.13902

## PRESENTATIONS:

**Mayer, K.**, Verjan-Garcia, N., & Matoba, N. (2023, October). “Avaren-Fc: A Novel Antibody-Based Immunotherapy Targeting High-Mannose Glycans for Ovarian Cancer Treatment.” Presented at Research! Louisville, Louisville, KY. 1<sup>st</sup> place poster award in Master’s Basic Science Graduate Student Category.

**Mayer, K.**, Verjan-Garcia, N., & Matoba, N. (2023, September). “Avaren-Fc: A Novel Antibody-Based Immunotherapy Targeting High-Mannose Glycans for Ovarian Cancer Treatment.” Presented at the Brown Cancer Center Retreat, Louisville, KY.

**Mayer, K.**, Verjan-Garcia, N., & Matoba, N. (2023, March). “Characterization of a High-Mannose-Binding Lectibody as a Novel Anti-Ovarian Cancer Therapeutic.” Presented at the Graduate Student Regional Research Conference, Louisville, KY.

**Mayer, K.**, Dent, M., & Matoba, N. (2021, October). “Anti-Ovarian Cancer Activity of a Lectibody Targeting Tumor-associated High-Mannose Glycans.” Presented at Research! Louisville, Louisville, KY.

**Mayer, K.**, Dent, M., & Matoba, N. (2021, July). “Anti-Ovarian Cancer Activity of a Lectibody Targeting Tumor-associated High-Mannose Glycans.” Presented at the NCI R25 poster session, Louisville, KY.

Fischbach, A., **Mayer, K.**, Becerra, A., & Mervis, C. (2021, April). “Relations between maternal language input and child language development for children with Williams syndrome.” Presented at the Gatlinburg Conference on Research and Theory in Intellectual and Developmental Disabilities, Kansas City, MO.

## MENTORING:

2 undergraduate students - National Cancer Institute R25 Cancer Education Program

1. Collins, K., Santisteban-Celis, I., **Mayer, K.**, & Matoba, N. (2022). “The Purification and Development of a Lectikine Targeting Tumor-associated High-Mannose Glycans.” – 1<sup>st</sup> place NCI R25 poster presentation.

2. Vemuri, S., **Mayer, K.**, & Matoba, N. (2023). "Avaren-Fc, a Novel Immunotherapeutic, Recruits NK Cells in B16F10 Melanoma Tumor Tissue." – 2<sup>nd</sup> place Brown Cancer Center Undergraduate poster presentation, 2<sup>nd</sup> place NCI R25 poster presentation.

EMPLOYMENT:

Research Technician I, Brown Cancer Center

2021-2022